Monthly Notices
of the
ROYAL ASTRONOMICAL SOCIETY

MNRAS **453,** 1439–1457 (2015) doi:10.1093/mnras/stv1596

The observed distribution of spectroscopic binaries from the Anglo-Australian Planet Search

J. S. Jenkins,[1]★ M. Díaz,[1] H. R. A. Jones,[2] R. P. Butler,[3] C. G. Tinney,[4,5] S. J. O'Toole,[6] B. D. Carter,[7] R. A. Wittenmyer[4,5] and D. J. Pinfield[2]

[1]*Departamento de Astronomía, Universidad de Chile, Casilla 36-D, Las Condes, Santiago, Chile*
[2]*Centre for Astrophysics Research, University of Hertfordshire, College Lane, Hatfield, Herts AL10 9AB, UK*
[3]*Carnegie Institution of Washington, DTM, 5241 Broad Branch Road NW, Washington, DC 20015-1305, USA*
[4]*Exoplanetary Science at UNSW, School of Physics, UNSW Australia, Sydney, NSW 2052, Australia*
[5]*Australian Centre for Astrobiology, UNSW Australia, Sydney, NSW 2052, Australia*
[6]*Australian Astronomical Observatory, PO Box 915, North Ryde, NSW 1670, Australia*
[7]*Computational Engineering and Science Research Centre, University of Southern Queensland, Springfield, QLD 4300, Australia*

Accepted 2015 July 14. Received 2015 July 10; in original form 2015 January 25

ABSTRACT

We report the detection of sixteen binary systems from the Anglo-Australian Planet Search. Solutions to the radial velocity data indicate that the stars have companions orbiting with a wide range of masses, eccentricities and periods. Three of the systems potentially contain brown-dwarf companions while another two have eccentricities that place them in the extreme upper tail of the eccentricity distribution for binaries with periods less than 1000 d. For periods up to 12 years, the distribution of our stellar companion masses is fairly flat, mirroring that seen in other radial velocity surveys, and contrasts sharply with the current distribution of candidate planetary masses, which rises strongly below 10 M_J. When looking at a larger sample of binaries that have FGK star primaries as a function of the primary star metallicity, we find that the distribution maintains a binary fraction of $\sim$43 $\pm$ 4 per cent between -1.0 and $+0.6$ dex in metallicity. This is in stark contrast to the giant exoplanet distribution. This result is in good agreement with binary formation models that invoke fragmentation of a collapsing giant molecular cloud, suggesting that this is the dominant formation mechanism for close binaries and not fragmentation of the primary star's remnant protoplanetary disc.

Key words: catalogues – binaries: spectroscopic – brown dwarfs – stars: fundamental parameters – stars: solar-type.

1 INTRODUCTION

Binary systems, in their various guises, yield vital measures for a range of fundamental parameters – mass, radius, luminosity – for the component stars. Studies of the binary population distribution, correlation of orbital elements, and the frequencies of the various forms of multiplicity, can be used to shed light on star formation processes and evolutionary mechanisms. Systems comprising two or more stars are common. Surveys suggest the incidence of multiplicity is around 45 per cent (Raghavan et al. 2010), perhaps higher than 70 per cent among the more massive stars (Abt, Gomez & Levy 1990; Mason et al. 1998; Preibisch et al. 1999), and somewhat lower ($\sim$30–40 per cent) for M dwarfs (Fischer & Marcy 1992).

Doppler searches for extrasolar planets have refined the art of single-lined spectroscopic binary analysis to the point where *relative* radial velocities (RVs) of the primaries can be measured with precisions at the $\sim$1 m s^{-1} level using both the absorption cell and spectrograph stabilization methods (e.g. Vogt et al. 2010; Jenkins et al. 2013b; Anglada-Escudé et al. 2014; Jenkins & Tuomi 2014; Wittenmyer et al. 2014). RV measurements that are not tied to an absolute zero-point can achieve high internal precision by explicitly removing the need to quantify such effects as convective blueshift and stellar gravitational redshift; a clear account of these and other effects is given in Nidever et al. (2002). The target stars for such planetary searches are generally solar-type and are selected to be chromospherically 'quiet' in order to minimize the potential for 'noise' in any velocity measurement due to star-spot activity (see Jenkins et al. 2006). They are also selected to have no resolvable companions to avoid flux contamination.

The Anglo-Australian Planet Search (AAPS) selection criteria for its initial group of stars are discussed in Jones et al. (2002b). The sample considered here comprises 178 F, G, and K dwarf stars with declinations south of $\sim -20^\circ$ and is complete to $V < 7.5$. There

★ E-mail: jjenkins@das.uchile.cl

Table 1. The primaries: stellar characteristics.

	Star	$B-V$	V	Parallax (mas)	M_V	Spectral type	[Fe/H] Casa	[Fe/H] Bond	$\log R'_{\rm HK}$	Mass ($M_\odot$)
1	HD 18907	0.79	5.9	31.1	3.4	K2V	−0.46	−0.50 ± 0.07	−5.11	1.05 ± 0.15
2	HD 25874	0.67	6.7	38.6	4.6	G2V	−0.02	–	−4.95	1.00 ± 0.05
3	HD 26491	0.64	6.4	42.3	4.5	G1V	−0.11	−0.08 ± 0.07	−4.95	0.97 ± 0.05
4	HD 39213	0.81	9.0	16.3	5.1	K0V	–	0.20 ± 0.07	−5.10	0.93 ± 0.05
5	HD 42024	0.55	7.2	18.2	3.5	F7V	0.19	–	–	1.30 ± 0.05
6	HD 64184	0.68	7.5	30.0	4.9	G3V	−0.18	−0.23 ± 0.07	−4.88	0.93 ± 0.05
7	HD 120690	0.70	6.4	51.4	5.0	G5+V	−0.08	−0.10 ± 0.06	−4.78	0.98 ± 0.05
8	HD 121384	0.78	6.0	25.8	3.1	G8V	−0.39	−0.40 ± 0.07	−5.22	0.98 ± 0.10
9	HD 131923	0.71	6.3	41.9	4.4	G4V	0.06	−0.05 ± 0.08	−4.90	1.05 ± 0.05
10	HD 145825	0.65	6.6	46.4	4.9	G3V	0.12	−0.04 ± 0.07	−4.74	1.03 ± 0.05
11	HD 150248	0.65	7.0	37.5	4.9	G3V	−0.13	−0.11 ± 0.07	−4.88	0.93 ± 0.05
12	HD 156274B	0.76	5.5	113.6	5.8	G8V	−0.40	–	−4.95	0.83 ± 0.06
13	HD 158783	0.67	7.1	23.7	4.0	G4V	0.05	−0.05 ± 0.07	−4.91	1.04 ± 0.05
14	HD 162255	0.66	7.2	24.9	4.2	G3V	0.17	−0.01 ± 0.08	–	1.12 ± 0.08
15	HD 169586	0.55	6.8	21.4	3.5	G0V	0.32	–	−4.92	1.25 ± 0.05
16	HD 175345	0.57	7.4	21.3	4.0	G0V	−0.16	–	–	1.05 ± 0.05

is a requirement that the activity seen in Ca II H&K absorption lines has an index (measured by log $R'_{\rm HK}$ – hereafter referred to as $R'_{\rm HK}$; for details see Jenkins et al. 2006, 2008, 2011) of less than −4.5, and for there to be no known companions within 2 arcsec. The spectroscopic binaries presented in this paper are drawn from this sample.

2 OBSERVATIONS AND DATA REDUCTION

2.1 The primaries: stellar characteristics

A summary of the characteristics and masses for the primaries are given in Table 1. Spectral types, $B-V$ colours, magnitudes, and parallaxes for all the stars are taken from the SIMBAD and HIPPARCOS data bases. Metallicities for the stars in this sample are drawn from two sources; spectroscopic metallicities were extracted from Bond et al. (2006) and photometric values were taken from the catalogue of Casagrande et al. (2011). For five of the binary stars we report there are no Bond et al. (2006) spectroscopic values; however, these have Casagrande et al. (2011) metallicities. In fact, all but one of the primaries, HD 39213, have Casagrande et al. (2011) measurements, allowing for a uniform and self-consistent set of [Fe/H] estimates to be generated for the sample.

$R'_{\rm HK}$ data are used with the activity–age relation given in Soderblom, Duncan & Johnson (1991) to provide secondary age estimates for the stars. Note that since our stars were preselected to have $R'_{\rm HK}$ values below −4.5, the Soderblom et al. relations are quantitatively the same in this regime to the updated work of Mamajek & Hillenbrand (2008) due to the sparse activity–age data for older dwarf stars. The activity values have been drawn from the studies of Henry et al. (1996), Tinney et al. (2002), Jenkins et al. (2006), and Jenkins et al. (2011), yet even considering these four works, there are still three stars with unknown activities, highlighting the lack of chromospheric activity studies in the Southern hemisphere compared to the north. The primary stellar ages, along with the stellar masses, are determined through interpolation of the Yonsei–Yale isochrones (Yi et al. 2001) and uncertainties can be found to reach 100 per cent for the ages of these types of old and Sun-like dwarf stars. Given the ∼0.06–0.10 dex uncertainty in metallicities, natural variations in stellar activity (for example solar $R'_{\rm HK}$ activity variation between –4.75 and –5.10 translates to an age variation from 2.2 and 8.0 Gyr; Henry et al. 1996), uncertainty in the precise form of the age–activity relationship, along with the possibility of flux contamination from the secondary, a number of isochronal mass/age/metallicity points can equally account for a star's colour and magnitude. In fact, an offset is found between ages derived from the activity indices and those measured from isochrone fitting, whereby the activity derived ages are generally significantly younger than those measured from fitting the isochrones. This result highlights that more work is needed to make ages derived from stellar activity relations, or gyrochronology, and those derived from evolutionary models, more consistent for old field stars. A consideration of these uncertainties enables us to determine a consistent mass range for each star.

2.2 Determination of RVs

2.2.1 UCLES data

Observations were made at the 3.9m Anglo-Australian Telescope using the University College London Echelle Spectrograph (UCLES), operated in its 31 lines/mm mode. High-precision Doppler measurements are made possible by the use of an iodine absorption cell that permits detailed modelling of the spectrograph point spread function (PSF). The reader is referred to Butler et al. (1996, 2001) for a detailed description, however, the procedure is outlined below.

Multi-epoch spectra at a resolution of $R \sim 45\,000$ are obtained for each star with the I_2 cell mounted behind the UCLES, imprinting the stellar spectra with thousands of iodine absorption lines in the 5000–6200 Å region. Each spectrum can be synthesized from a product of a Doppler-shifted copy of a pure stellar spectrum for the star in question (a higher resolution stellar *template* spectrum from which the spectrograph PSF has been removed) and an iodine absorption spectrum, all of which is convolved with the spectrograph's PSF at the time of the observation. A least-squares fitting process matches this synthetic spectrum with the observed spectrum, and determines up to 14 free parameters (one being the Doppler shift, one the wavelength dispersion, and the remainder associated with the detailed PSF profile). This fitting process is carried out on 2 Å chunks of the spectrum between 5000 and 6200 Å and the resulting velocities are weighted by the gradient ($\partial F/\partial\lambda$) of the spectral

profile for each chunk. The mean of these weighted velocities, corrected for the Earth's motion relative to the Solar system barycentre (McCarthy 1995), represents the RV for that observation. A barycentric correction is also applied to the Julian dates. The internal uncertainty is obtained from the standard deviation of the velocities. This technique has demonstrated consistently that 3 m s^{-1} precision is achievable down to the $V = 7.5$ mag limit of the survey for suitably inactive stars over the long term (Jones et al. 2002a). The barycentric Julian dates and RV data of our sources are given in Table 3.

2.2.2 *HARPS data*

In order to supplement the velocities measured using the UCLES spectrograph, we performed a search of the ESO Archive Facility to determine if any of these stars had high-precision ESO-HARPS measurements that could be used to increase the phase coverage of our orbits. The search revealed that six of targets had been observed with HARPS multiple times, such that the inclusion of the velocities yielded much better constraints on the binary orbits. The HARPS RV data are also shown in Table 3.

At this point it is worth briefly discussing the HARPS strategy for measuring precision RVs from high-resolution and high S/N echelle spectra. The HARPS data are automatically processed by the HARPS-DRS version 3.5, with the reduced and analysis quality data on the Advanced Data Products page of the ESO Archive website. The actual reduction and analysis method itself is based in general on the procedure explained in Baranne et al. (1996). Unlike the method employed by the AAPS using UCLES, no iodine cell is used by HARPS, but instead, precision RVs are measured by maintaining the highest stability possible over the long term, but placing the spectrograph in a vacuum tank to maintain the pressure and temperature as stable as possible, and feeding the light to the spectrograph using optical fibres.

The actual RV measurements are not performed in chunks like they are using UCLES, but each entire echelle order is used to measure the RV. A weighted binary mask is constructed that synthetically mimics the position of an absorption line in the star (Pepe et al. 2002), and a weighted cross-correlation between the stellar spectrum and the binary mask gives the RV. The mean of the RV for each order gives rise to the final absolute RV measurement from the star, with the uncertainty measured following the procedure in Bouchy, Pepe & Queloz (2001). The stability of the spectrograph is maintained by using a calibration Thorium–Argon lamp, that is also simultaneously fed to the spectrograph using another fibre, allowing any drifts in the wavelength solution to be measured at the 0.1 m s^{-1} level (Lovis & Pepe 2007). The drift is then removed from the measured RV to get the most precise value; however, a stability of less than 1 m s^{-1} has been found for HARPS data over the long term (e.g. Lo Curto et al. 2010).

2.3 Orbital parameters

For the analysis of spectroscopic binaries the task is to provide a set of orbital parameters (period, P, eccentricity, e, periastron angle, ω, time of periastron passage, $T_{\rm p}$, and the projected semimajor axis of the primary, $a_{\rm p}\,sin\,{\rm i}$) – and a velocity offset, $\dot{z}_{\rm o}$, that optimize the fit of the equation

$$\dot{z} = \frac{2\pi a_{\rm p} \sin i}{P\sqrt{1-e^2}}(\cos(\upsilon+\omega) + e\cos\omega) + \dot{z}_{\rm o} \qquad (1)$$

to the n observations of line-of sight RV, $\dot{z}$, at true anomalies υ (derived from the observed times, t, through iteration of Kepler's equation). A least-squares minimization procedure, invoking several IDL routines, is used to fit the equation.

In the search for an orbital solution, periods are initially identified via Lomb–Scargle periodogram analysis (Lomb 1976; Scargle 1982). Orbital solutions are plotted in Fig. 1 and summarized in Table 2 (i and ii). Where the RV data have a monotonic variation, or only one extremum occurs without any clear inflection in the RV variation to constrain a second extremum (HD 18907, HD 25874, HD 26491, HD 131923, HD 156274B), convergence is reached for a number of different periods. In these cases, where the period is clearly greater than the duration of the observations, and where periodogram analysis is least effective, we consider only the minimum orbital period in our solutions. Periodograms are shown (Fig. 2) for all the targets where the RV phase coverage is nearly a cycle or more. Where the sampling is sparse, aliasing introduces spectral power over a range of frequencies and is particularly marked for HD 64184 which has just eight RV observations and for HD 121384 due to the highly eccentric nature of the orbit (see O'Toole et al. 2009). This is perhaps a reminder that data sets should comprise more than a dozen observations for the periodogram technique to be properly effective (Horne & Baliunas 1986). The period inferred from the orbital solution in each case is marked with a vertical dashed line. Identification of periods is least effective for HD 131923 and HD 156274B, where the phase coverage is less than one cycle. Nevertheless, the inflections in the RV variation enable a robust Keplerian period to be found.

3 DISCUSSION

3.1 The binary stars

HD 18907: A high proper-motion star classed as K2 V (Gray et al. 2006) though consistently classified as a G5 IV prior to this (e.g. Evans, Menzies & Stoy 1957), its colour and magnitude confirm that it is evolving away from the main sequence. Chromospherically quiet ($R'_{\rm HK}$= −5.11, Jenkins et al. 2006), HD 18907 is most likely an old star with an age in excess of 12 Gyr which agrees with isochrone fits based on metallicities derived through spectral and photometric analysis – for example [Fe/H] = −0.50 dex from Bond et al. (2006) and −0.46 dex from Casagrande et al. (2011). This age/metallicity scenario translates to a stellar mass estimated to be 1.05 M$_\odot$. Limited phase coverage of the RV data means that the period is not well constrained so the orbital solution converges to a number of fits with periods upwards of 10 000 d. The shortest period orbit translates to a secondary minimum mass ($M_{\rm s}\,\sin i$) of 0.42 ± 0.10 M$_\odot$.

HD 25874: Classified as a G2V by Gray et al. (2006) and listed by (Dommanget & Nys 1994) in the Catalogue of Components of Double and Multiple Stars, it is identified along with a $V = 12$ companion (position angle 225°, separation 29 arcsec, 1941) as a common proper-motion pair. Jenkins et al. derive an $R'_{\rm HK}$ index of −4.95, suggesting an age of about 4 Gyr, while Casagrande et al. (2011) find a metallicity of [Fe/H] = −0.02 dex, suggesting an age of 9.2 Gyr, in agreement with the sub-giant designation. Given the age–metallicity range, a mass of 1.00 ± 0.05 M$_\odot$ is inferred for the primary. Since the phase coverage from both the AAPS and HARPS is limited, a variety of solutions exist; however, we find that the best solution to the data gives rise to a very long-period low-mass stellar companion, with a period of nearly 200 years and a minimum mass of 0.33 ± 0.07 M$_\odot$.

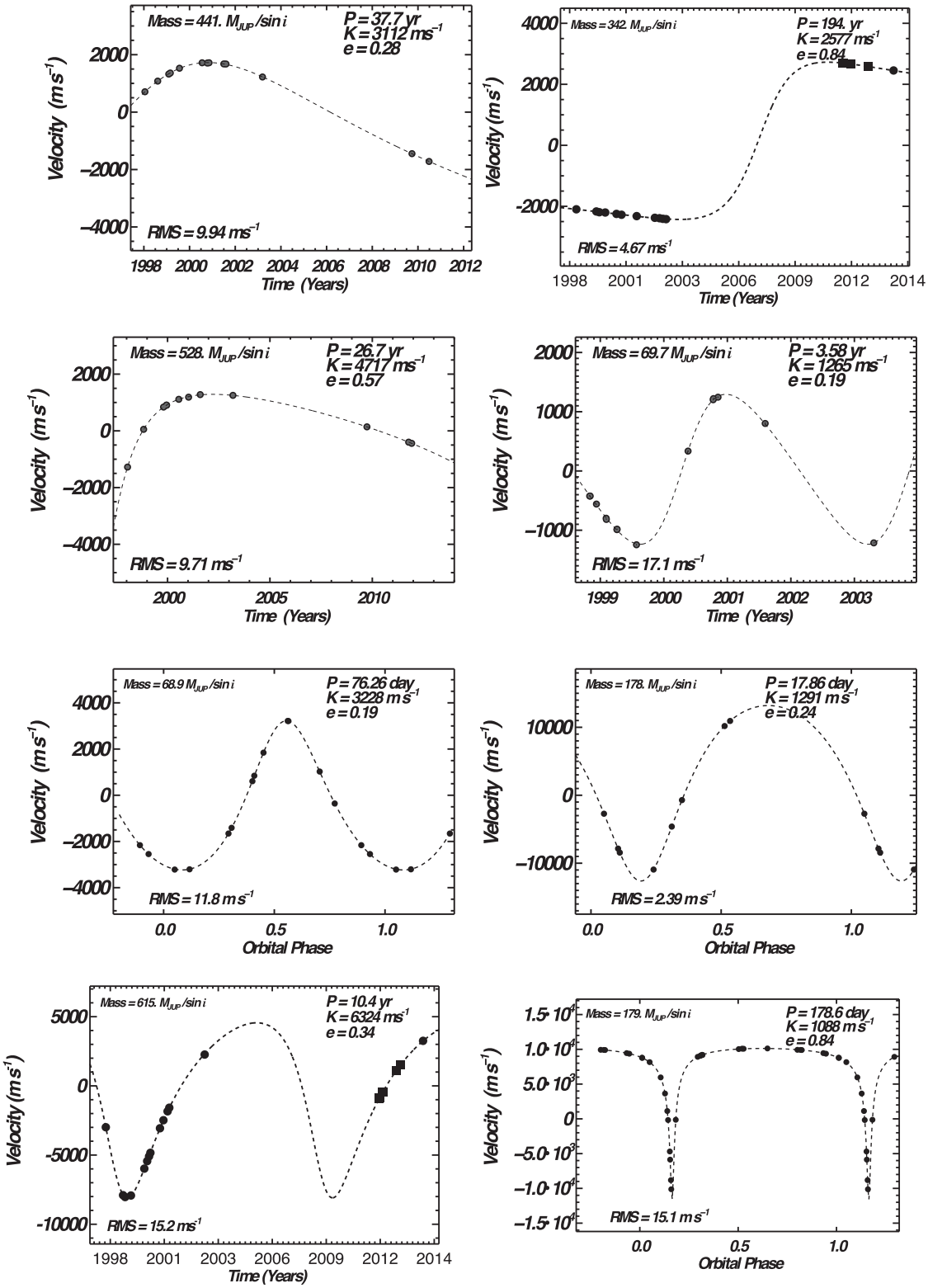

Figure 1. RV curves for our stars, with filled circles representing data from the AAPS and filled squared data from HARPS. From top left to bottom right we show the stars in catalogue order, HD 18907, HD 25874, HD 26491, HD 39213, HD 42024, HD 64184, HD 120690, HD 121384, respectively. From top left to bottom right we show the stars in catalogue order, HD 131923, HD 145825, HD 150248, HD 156274B, HD 158783, HD 162255, HD 169586, and HD 175345, respectively.

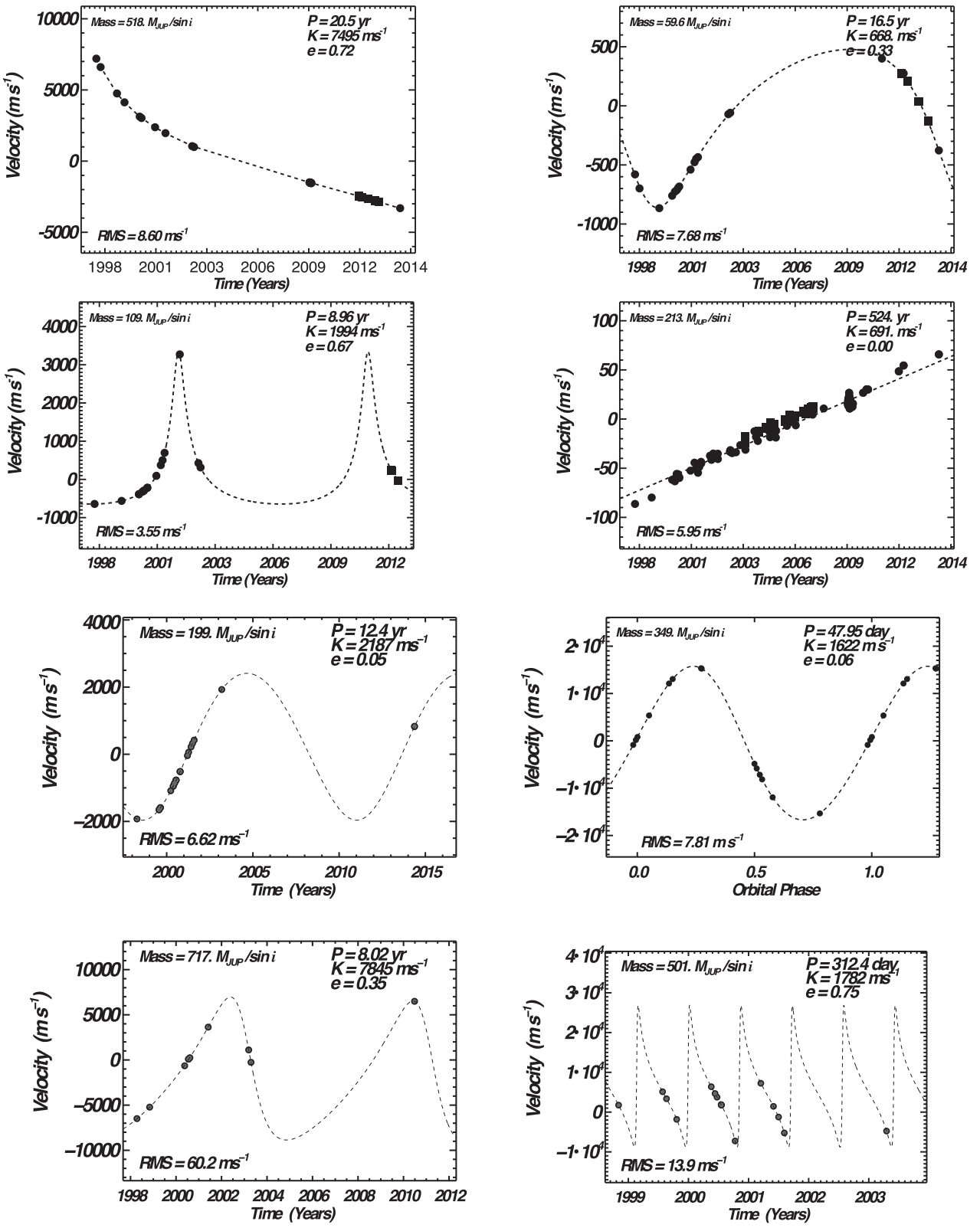

Figure 1 – *continued*

HD 26491: This is classified as a G1V by Gray et al. (2006), and previously consistently classified as a G3 (Houk & Cowley 1975; Evans 1964), and is identified by Decin et al. (2000) as having a Vega-like IR excess. Bond et al. (2006) derive a spectroscopic metallicity of [Fe/H] = −0.08 dex, which is larger than the Casagrande et al. (2011) value of −0.11 dex. An age of 10.5 Gyr is indicated by the isochrone fit which is somewhat older than the 5 Gyr inferred from an $R'_{\rm HK}$ index of −4.95 (Henry et al. 1996). Accordingly a mass of 0.97 ± 0.05 $M_\odot$ is assigned to this high proper-motion star. Given the nature of the RV variation (Fig. 1), orbital solutions

Table 2. (i) Orbital parameters 1: where the RV data extend over more than one cycle or a clear inflection in the RV variation is seen to be able to constrain a second extremum, a single set of orbital parameters emerge and are listed below. The quantity $a \sin i$ represents the semimajor axis of the binary system.

Star	P (d)	ω (deg)	e	T_p JD− 2450000	K (m s^{-1})	a (au)	χ^2_υ	rms (m s^{-1})
HD 39213	1309 ± 159	265 ± 23	0.2 ± 0.1	1636.7 ± 2.8	1265 ± 273	2.3 ± 0.3	1.97	17.1
HD 42024	76.26 ± 0.03	347 ± 87	0.19 ± 0.01	1154.8 ± 0.7	3228 ± 133	0.38 ± 0.01	3.22	11.8
HD 64184	17.863 ± 0.002	184 ± 84	0.249 ± 0.004	949.50 ± 0.05	12 910 ± 439	0.130 ± 0.002	0.93	2.39
HD 120690	3800 ± 18	339 ± 55	0.34 ± 0.01	1140 ± 11	6325 ± 100	4.73 ± 0.02	27.7	15.2
HD 121384	178.7 ± 0.1	182 ± 28	0.84 ± 0.01	852 ± 1	10 887 ± 2201	0.61 ± 0.02	7.19	15.1
HD 150248	3272 ± 29	356 ± 68	0.67 ± 0.04	2365 ± 13	1995 ± 12	4.36 ± 0.01	3.19	3.55
HD 158783	4535 ± 225	170 ± 46	0.05 ± 0.05	986 ± 27	2133 ± 527	5 ± 1	3.03	6.62
HD 162255	48 ± 1	51 ± 5	0.06 ± 0.01	1017.1 ± 0.1	16 223 ± 3419	0.27 ± 0.01	2.49	7.81
HD 169586	2935 ± 119	59 ± 10	0.4 ± 0.1	2653 ± 22	7857 ± 2708	4.3 ± 0.2	11.5	60.2
HD 175345	312.4 ± 0.1	277 ± 14	0.75 ± 0.05	1256 ± 11	16 099 ± 3675	0.92 ± 0.01	3.44	13.9

Table 2. (ii) Orbital parameters 2: where the RV data have a monotonic variation, or only one extremum occurs without any clear inflection in the RV variation to constrain a second extremum, a number of solutions emerge at different periods. For each system we list the orbital parameters for the 'best-fitting' solution having the shortest period. The associated uncertainties are for this fit.

Star	P_{min} (d)	ω (deg)	e	T_p JD− 2450000	K (m s^{-1})	a (au)	χ^2_υ	rms (m s^{-1})
HD 18907	13 770 ± 3528	314 ± 34	0.28 ± 0.07	865 ± 9	3112 ± 1903	13 ± 4	4.31	9.94
HD 25874	71 108 ± 2308	274 ± 10	0.8 ± 0.1	4382 ± 2453	2578 ± 253	33 ± 2	4.16	4.67
HD 26491	9748 ± 1223	221 ± 38	0.57 ± 0.05	250.9 ± 0.5	4717 ± 2969	10 ± 2	3.16	9.71
HD 131923	7495 ± 334	15 ± 79	0.72 ± 0.02	528 ± 30	5784 ± 821	8.7 ± 0.4	21.8	8.60
HD 145825	6024 ± 163	149 ± 53	0.33 ± 0.02	1095 ± 13	669 ± 10	6.54 ± 0.04	14.4	7.68
HD 156274B	191 455 ± 13 707	30 ± 85	0.0 ± 0.1	5222 ± 10 588	692 ± 55	63.5 ± 0.2	11.4	5.95

with periods significantly longer than ∼7000 d are possible, and in all cases the eccentricity is greater than ∼0.5. An orbital period of 9747.5 ± 1223.2 d ($e = 0.57$) translates to a secondary minimum mass of 0.50 ± 0.15 $M_\odot$.

HD 39213: The Bond et al. (2006) metallicity of this K0 dwarf (Houk 1982) is found to be [Fe/H] = 0.20 ± 0.07 dex. The measured R'_{HK} index of −5.10 relates to an age of 8 Gyr and by fitting a range of isochrones with ages from 7.5 and 10 Gyr, respectively, a mass range of 0.93 ± 0.05 $M_\odot$ is inferred. Though the orbital parameters appear tightly defined (helped by the RV data having a phase coverage close to one cycle), the residuals are relatively high (rms = 17.1 m s^{-1}) and the χ^2_υ of 1.97 suggests the fit is significant at under the 5 per cent level. A Keplerian period of ∼1300 d and eccentricity of ∼0.2 translate to a companion with a minimum mass of 0.07 ± 0.01 $M_\odot$ – potentially a brown dwarf if the orbit is being seen close to edge on.

HD 42024: Given a Casagrande et al. (2011) metallicity of 0.19 for this star, isochrones ranging in age from 2.5–4 Gyr suggest a mass of 1.30 ± 0.05 $M_\odot$ for this F7 dwarf (Houk 1978), though the lack of an R'_{HK} index deprives us of a secondary age indicator. Phase coverage is broad and the RV values fold convincingly around a period of 76.26 d (Fig. 1) with well-defined orbital parameters to yield a companion minimum mass of 0.066 ± 0.003 $M_\odot$, another possible brown dwarf companion. Residuals are above average with an rms for the fit of 11.8 m s^{-1}.

HD 64184: This G3 dwarf (Gray et al. 2006) is listed in SIMBAD as a variable ($V = 7.49$–7.55), though no variability flag is marked in HIPPARCOS. The Bond et al. (2006) and Casagrande et al. (2011) metallicities are in close agreement at −0.23 and −0.18 dex, respectively, and an age between 7–10 Gyr is indicated by the isochrone fits, somewhat older than the ∼4 Gyr inferred from the R'_{HK} index (−4.88; Henry et al. 1996). The stellar mass is estimated at 0.9 ± 0.1 $M_\odot$. The eight RV measurements fold convincingly around a period of 17.86 d (Fig. 1) and the orbital parameters, which are tightly defined by the broad phase coverage, suggest a companion with an $M_s \sin i$ of 0.170 ± 0.001 $M_\odot$ and an orbital separation of 0.130 ± 0.002 au. With a sufficiently high orbital inclination (≥87°), the secondary could provide sufficient obscuration of the primary's surface for a variation in V of ± 0.03 mag, given that a mass of 0.160 $M_\odot$ would be no brighter than $M_V \sim 9.6$ at 6 Gyr – (Baraffe et al. 1998).

HD 120690: This G5+V, as classified by Gray et al. (2006), has an R'_{HK} index of −4.78 (Henry et al. 1996), equivalent to an age of ∼3 Gyr. Metallicities are found to be −0.10 and −0.08 dex from Bond et al. (2006) and Casagrande et al. (2011), respectively, suggesting an age from the isochrone fits somewhere between 6.5 and 9 Gyr, from which a stellar mass of 0.98 ± 0.05 $M_\odot$ is inferred. While limited phase coverage of RV data means that the orbital period is only poorly constrained by periodogram analysis (1900 ± 500 d), a full orbital solution yields tightly defined parameters. A Keplerian period of 3799.98 ± 18.12 d and an eccentricity of 0.34 indicate a secondary minimum mass of 0.59 ± 0.01 $M_\odot$. With the secondary contributing upwards of ∼0.4 per cent of the flux at 5500 Å, the central region over which RVs are determined, contamination of the primary spectrum could be a contributory factor. It could also affect the star's colour–magnitude location making it appear redder (and apparently more evolved) possibly accounting for an element of the age discrepancy mentioned above. These issues are considered further in Section 3.4. We do note that a second signal may be present in the data, with a period of 531 d and a

Table 3. UCLES and HARPS RV data for all stars discussed in this work.

HD 18907	Instrument	Date (JD − 2450000)	RV ($m\,s^{-1}$)	RV error ($m\,s^{-1}$)
	UCLES	831.050 35	−616.2	1.8
		1035.325 46	−245.1	1.4
		1211.969 92	0.00	2.3
		1236.912 35	36.6	2.1
		1383.332 60	203.4	1.4
		1745.299 74	393.0	1.6
		1828.116 60	383.8	2.6
		1856.113 91	393.7	2.6
		2092.289 43	353.0	1.6
		2127.248 66	350.0	2.5
		2710.886 87	−101.4	2.1
		5101.255 80	−2772.4	1.3
		5374.327 32	−3044.1	1.2
HD 25874	Instrument	Date (JD − 2450000)	RV ($m\,s^{-1}$)	RV error ($m\,s^{-1}$)
	UCLES	1118.122 18	−1005.7	1.5
		1473.261 27	−551.9	1.9
		1526.013 61	−499.2	1.6
		1630.876 12	−353.4	1.7
		1830.117 89	−105.3	2.1
		1920.037 98	0.0	2.0
		2189.176 94	352.8	3.0
		2511.239 25	773.4	4.3
		2594.080 90	882.2	2.8
		2654.061 84	950.8	2.2
		2710.891 86	1024.2	2.4
		6746.883 41	11860.0	5.2
	HARPS	5846.822 36	2700.0	2.1
		5846.827 32	2701.3	2.1
		5850.828 95	2699.5	2.1
		5850.833 81	2698.9	2.1
		5851.815 10	2698.4	2.1
		5851.820 11	2698.8	2.1
		5852.814 06	2697.6	2.1
		5852.818 97	2697.2	2.1
		5984.509 42	2669.3	2.0
		5984.514 41	2669.2	2.1
		5986.535 69	2668.6	2.0
		5986.540 65	2668.6	2.0
		6298.598 13	2585.0	2.1
		6298.603 23	2585.8	2.1
		6301.617 64	2587.3	2.1
		6301.622 50	2585.5	2.1
		6746.880 00	2453.6	5.2
HD 26491	Instrument	Date (JD − 2450000)	RV ($m\,s^{-1}$)	RV error ($m\,s^{-1}$)
	UCLES	831.076 78	−2115.6	1.5
		1118.136 48	−784.2	1.6
		1473.264 23	0.0	2.0
		1525.977 09	70.9	1.8
		1527.062 95	65.8	1.8
		1745.328 14	274.1	1.9
		1920.043 74	349.3	3.3
		2127.302 80	439.6	3.0
		2710.897 27	413.5	1.8
		5101.202 38	−697.0	1.3
		5845.248 38	−1236.9	2.9
		5899.071 15	−1278.6	2.3

Table 3 – *continued*

HD 39213	Instrument	Date (JD − 2450000)	RV ($m\,s^{-1}$)	RV error ($m\,s^{-1}$)
	UCLES	1118.212 33	13.2	5.9
		1121.176 19	12.6	7.6
		1157.150 34	−122.2	8.1
		1212.990 66	−361.0	8.0
		1214.091 91	−381.4	7.5
		1274.869 86	−553.7	7.5
		1275.870 68	−545.8	8.2
		1387.334 31	−809.0	10.9
		1683.855 61	772.0	10.6
		1828.198 55	1638.4	9.1
		1830.045 17	1657.9	12.6
		1856.2322	1681.6	9.5
		2127.333 54	1238.2	19.1
		2751.876 83	−777.0	6.8
HD 42024	Instrument	Date (JD − 2450000)	RV ($m\,s^{-1}$)	RV error ($m\,s^{-1}$)
	UCLES	1118.2294	−2859.2	8.0
		1157.166 31	3573.5	2.9
		1213.023 11	−1299.5	2.8
		1214.100 00	−1052.7	2.7
		1275.878 45	−2848.1	3.5
		1411.312 72	−1804.3	5.8
		1414.300 77	−2188.3	2.5
		1473.239 53	1382.8	2.8
		1530.150 77	2200.9	3.1
		1630.952 38	0.0	3.2
		1920.069 37	3570.0	3.3
		1983.931 73	964.8	3.4
		2060.844 24	1201.9	2.9
HD 64184	Instrument	Date (JD − 2450000)	RV ($m\,s^{-1}$)	RV error ($m\,s^{-1}$)
	UCLES	946.852 78	0.0	2.7
		1236.063 03	−8217.3	2.8
		1630.998 29	2005.9	2.0
		1683.888 73	−1894.8	1.9
		1920.111 22	13 652.9	2.8
		1983.994 41	−5721.9	3.5
		2009.048 58	12 902.0	2.9
		2751.988 69	−5134.5	2.4
HD 120690	Instrument	Date (JD − 2450000)	RV ($m\,s^{-1}$)	RV error ($m\,s^{-1}$)
	UCLES	917.110 28	81.0	3.7
		1236.243 32	−4831.4	3.1
		1275.124 58	−4967.8	4.0
		1382.948 87	−4855.0	2.5
		1630.263 44	−2914.8	2.7
		1683.064 32	−2373.5	2.9
		1717.961 27	−2028.6	2.8
		1743.009 61	−1771.8	2.8
		1920.243 38	0.0	3.3
		1984.148 82	580.2	4.2
		2060.968 53	1224.4	3.4
		2092.974 58	1483.7	3.1
		2748.218 44	5322.1	5.5
		6793.066 82	6289.8	3.2
	HARPS	5983.859 98	−897.3	2.0
		5983.864 40	−898.1	2.1
		5984.842 68	−896.4	2.1
		5984.847 27	−893.5	2.1

Table 3 – *continued*

HD 120690	Instrument	Date (JD − 2450000)	RV (m s^{-1})	RV error (m s^{-1})
		5985.835 24	−889.2	2.1
		5985.839 71	−889.3	2.1
		5986.857 72	−877.0	2.1
		5986.862 06	−876.2	2.1
		6042.612 45	−472.6	2.1
		6042.616 87	−473.0	2.1
		6042.769 14	−472.1	2.1
		6042.773 48	−473.0	2.1
		6046.734 67	−446.5	2.1
		6046.738 70	−443.9	2.1
		6047.754 28	−439.1	2.1
		6047.758 62	−438.9	2.1
		6048.780 13	−435.9	2.1
		6048.784 67	−434.6	2.1
		6300.851 04	1104.6	2.1
		6300.855 51	1105.5	2.1
		6375.784 22	1515.5	2.0
		6375.788 65	1516.6	2.0
		6376.807 60	1515.1	2.1
		6376.812 02	1515.6	2.1
HD 121384	Instrument	Date (JD − 2450000)	RV (m s^{-1})	RV error (m s^{-1})
	UCLES	831.232 38	−761.1	1.2
		915.112 84	1173.1	2.2
		1002.942 45	−119.4	2.3
		1212.283 29	−9052.3	3.6
		1236.254 93	289.7	2.8
		1383.960 12	−9086.6	2.1
		1385.851 81	−14 785.4	2.3
		1386.864 23	−19 043.8	2.2
		1410.871 19	0.0	3.9
		1413.856 41	211.3	3.5
		1631.267 48	1160.1	2.4
		1682.991 33	992.2	3.0
		1684.068 55	980.7	2.8
		1706.076 67	451.6	3.3
		1717.833 28	−155.9	3.1
		1742.889 68	−13 609.7	2.8
		1743.881 68	−17 735.1	2.7
		1919.259 71	−7795.4	5.3
		1984.161 57	1114.1	2.3
		2010.266 83	1205.2	1.8
		2061.011 49	535.1	2.7
		2091.913 15	−2958.7	3.6
		2127.898 69	145.3	2.4
		2129.923 47	270.0	2.3
		2752.114 88	1007.9	1.1
		5669.184 15	−5277.9	0.8
HD 131923	Instrument	Date (JD − 2450000)	RV (m s^{-1})	RV error (m s^{-1})
	UCLES	831.266 15	8714.9	1.8
		915.141 55	8120.8	1.9
		1236.259 51	6268.9	2.5
		1383.980 96	5644.7	2.8
		1683.018 96	4640.8	2.3
		1718.057 74	4541.6	3.2
		1984.191 27	3894.3	2.2
		2187.864 19	3481.1	2.8
		2711.316 97	2566.7	3.5
		2748.221 62	2505.1	3.0
		5013.859 13	20.8	1.2

Table 3 – *continued*

HD 131923	Instrument	Date (JD − 2450000)	RV (m s^{-1})	RV error (m s^{-1})
		5017.879 36	18.0	1.1
		5018.990 94	13.0	1.0
		5019.966 96	14.7	1.1
		5020.908 13	6.1	1.4
		5021.912 60	7.3	1.4
		5023.906 83	−0.0	1.5
		5029.895 93	−3.4	1.2
		5030.850 82	−11.1	1.4
		5031.965 01	−2.9	1.1
		5032.995 08	−1.5	1.3
		5036.890 32	−13.7	1.3
		5037.888 30	−17.3	1.6
		5043.928 13	−24.9	1.3
		5044.875 81	−29.0	1.3
		5045.894 27	−25.5	1.1
		5048.903 80	−23.05	1.2
		5049.880 25	−26.0	1.7
		6793.098 17	−1791.3	2.5
	HARPS	5983.916 73	−1033.9	2.1
		5983.919 76	−1033.0	2.1
		5983.923 22	−1036.3	2.0
		5984.896 57	−1022.5	2.1
		5984.899 80	−1023.3	2.1
		5984.903 05	−1023.6	2.1
		5985.892 76	−1023.4	2.0
		5985.896 03	−1026.9	2.0
		5985.899 26	−1024.6	2.0
		6042.695 51	−1005.8	2.1
		6042.698 89	−1006.0	2.1
		6042.702 04	−1007.8	2.1
		6042.706 10	−1007.7	2.1
		6042.709 44	−1004.9	2.1
		6042.712 59	−1008.4	2.1
		6046.775 64	−1006.8	2.1
		6046.778 88	−1005.3	2.1
		6046.782 19	−1006.6	2.1
		6047.804 34	−1005.1	2.1
		6047.807 58	−1006.9	2.1
		6047.810 77	−1005.2	2.1
		6048.829 39	−1011.2	2.1
		6048.832 65	−1010.8	2.1
		6048.835 86	−1009.0	2.1
		6165.480 87	−961.2	2.0
		6165.484 09	−960.8	2.0
		6165.487 24	−960.9	2.0
		6299.841 38	−939.4	2.1
		6299.844 56	−940.9	2.1
		6300.875 69	−930.3	2.1
		6300.878 92	−931.1	2.1
		6300.882 22	−929.2	2.1
		6301.863 54	−927.0	2.1
		6301.866 87	−925.0	2.1
		6301.870 07	−926.2	2.1
		6375.838 88	−927.1	2.0
		6375.842 14	−926.0	2.0
		6375.845 38	−927.2	2.0
		6376.867 79	−928.7	2.1
		6376.871 02	−927.8	2.1
		6376.874 31	−928.3	2.1
		6377.794 62	−932.6	2.1
		6377.797 98	−930.0	2.1
		6377.801 19	−930.7	2.1

Table 3 – *continued*

HD 145825	Instrument	Date (JD − 2450000)	RV (m s^{-1})	RV error (m s^{-1})
	UCLES	915.181 78	−348.0	2.2
		1002.045 74	−448.0	3.0
		1382.973 83	−534.0	1.9
		1630.279 76	−375.7	2.0
		1683.046 91	−330.1	2.1
		1718.096 32	−310.8	2.2
		1742.997 28	−287.7	2.1
		1766.897 25	−269.1	1.8
		1984.223 96	−79.4	2.3
		2060.981 94	0.0	2.0
		2091.944 91	35.1	2.1
		2126.927 35	56.7	2.4
		2711.314 79	544.4	3.0
		2748.214 70	564.8	2.7
		5669.194 03	1646.1	1.8
		6088.207 21	1610.5	2.6
		6765.202 19	1103.0	1.2
	HARPS	6042.719 40	277.4	2.1
		6042.724 34	278.2	2.1
		6046.828 52	271.8	2.1
		6046.833 81	271.3	2.1
		6047.874 75	275.3	2.1
		6047.879 65	275.6	2.1
		6048.880 54	276.2	2.1
		6048.885 48	276.7	2.1
		6164.537 42	208.8	2.1
		6164.542 16	208.7	2.1
		6165.519 08	207.6	2.1
		6165.523 94	206.5	2.1
		6375.907 68	36.4	2.0
		6375.912 45	36.6	2.0
		6376.891 08	35.6	2.1
		6376.895 85	36.1	2.1
		6377.863 16	34.3	2.1
		6377.867 88	34.4	2.1
		6557.503 61	−128.5	2.4
		6557.508 34	−130.6	2.4
		6558.481 09	−131.0	2.1
		6558.485 82	−130.1	2.1
		6559.491 01	−128.4	2.1
		6559.495 73	−129.1	2.1
		6560.488 28	−126.6	2.1
		6560.493 00	−127.6	2.1

HD 150248	Instrument	Date (JD − 2450000)	RV (m s^{-1})	RV error (m s^{-1})
	UCLES	917.262 97	−506.1	3.0
		1384.036 61	−413.2	2.2
		1683.074 65	−229.2	2.3
		1684.123 07	−232.1	2.3
		1743.030 57	−164.5	2.1
		1766.914 99	−142.2	2.2
		1767.948 21	−134.0	2.4
		1827.890 80	−62.5	2.5
		1828.878 61	−54.9	2.2
		1984.239 53	259.2	2.7
		2061.090 80	541.6	2.3
		2091.963 33	670.8	2.0
		2126.951 64	865.5	2.0
		2389.211 41	3448.5	1.0
		2711.311 86	612.6	2.2
		2748.224 95	499.7	3.1

Table 3 – *continued*

HD 150248	Instrument	Date (JD − 2450000)	RV (m s^{-1})	RV error (m s^{-1})
	HARPS	6042.744 97	244.9	2.0
		6046.864 31	231.2	2.0
		6047.900 16	228.8	2.0
		6048.893 60	226.6	2.0
		6164.574 97	−24.5	2.1
		6165.555 98	−26.3	2.0

HD 156274B	Instrument	Date (JD − 2450000)	RV (m s^{-1})	RV error (m s^{-1})
	UCLES	915.251 03	−100.2	1.8
		1236.290 45	−93.6	1.9
		1631.312 56	−75.6	1.4
		1683.081 90	−77.1	1.9
		1684.130 26	−74.9	1.9
		1718.109 16	−69.6	1.6
		1743.972 23	−69.9	1.5
		1766.929 42	−72.9	1.7
		1767.963 59	−73.8	1.6
		1984.254 59	−66.3	1.8
		2061.105 43	−58.2	1.7
		2093.068 73	−64.4	1.7
		2127.965 61	−68.4	1.9
		2151.966 53	−62.5	1.8
		2186.906 47	−57.3	1.4
		2189.906 68	−58.9	1.3
		2359.213 66	−51.1	1.4
		2387.160 82	−54.1	1.4
		2388.202 99	−55.3	1.5
		2422.142 28	−48.9	1.3
		2455.031 40	−50.8	1.6
		2509.954 69	−49.0	1.7
		2510.921 82	−54.4	1.5
		2745.250 45	−47.2	1.6
		2746.306 57	−46.1	1.4
		2752.165 29	−45.4	1.6
		2784.118 07	−48.4	1.5
		2858.944 18	−47.6	1.6
		2942.923 55	−40.3	1.6
		3041.278 89	−38.1	1.7
		3042.290 99	−45.0	1.7
		3214.976 64	−26.2	1.5
		3245.006 97	−31.9	1.7
		3280.905 84	−36.0	1.5
		3483.235 36	−25.1	0.9
		3486.155 07	−24.5	0.7
		3507.146 09	−26.5	0.8
		3516.113 59	−32.2	1.0
		3517.152 45	−28.0	0.9
		3520.201 39	−22.4	0.9
		3521.183 10	−24.9	0.8
		3523.113 61	−21.8	0.8
		3569.028 20	−23.7	0.8
		3627.883 88	−32.6	1.1
		3628.915 53	−25.2	0.8
		3631.881 50	−25.8	0.7
		3842.226 56	−20.6	0.9
		3938.051 95	−12.5	0.8
		4010.912 05	−20.1	0.7
		4226.206 07	−7.9	1.0
		4255.005 36	−8.0	0.9
		4336.018 44	−9.2	1.1
		4550.263 95	−3.0	1.8
		5013.934 67	1.4	0.9

Table 3 – *continued*

HD 156274B	Instrument	Date (JD − 2450000)	RV ($m\,s^{-1}$)	RV error ($m\,s^{-1}$)
		5014.991 59	1.8	2.0
		5017.913 53	2.3	1.0
		5019.049 22	2.4	1.0
		5020.073 29	5.4	1.0
		5020.862 56	−0.2	1.0
		5021.996 21	4.5	0.9
		5023.004 47	1.6	1.1
		5024.008 43	7.2	0.9
		5027.068 74	6.2	0.9
		5029.961 15	3.1	1.0
		5030.129 74	5.3	0.9
		5030.915 09	1.8	0.8
		5032.045 41	4.7	0.9
		5032.967 09	5.4	0.9
		5036.969 46	9.2	0.8
		5039.019 74	13.0	0.8
		5040.006 08	10.5	1.4
		5043.971 42	8.1	0.7
		5044.969 94	5.0	0.9
		5046.867 56	5.4	0.6
		5047.971 02	3.8	0.9
		5049.064 88	1.7	0.7
		5049.949 76	1.6	0.9
		5050.945 61	−3.0	0.9
		5051.916 15	−1.7	0.9
		5052.940 01	−2.1	1.6
		5053.944 17	2.9	1.3
		5054.946 08	3.2	0.9
		5056.035 35	4.0	0.8
		5056.996 12	6.4	0.8
		5057.996 25	4.9	0.8
		5058.988 84	6.5	0.8
		5076.036 18	−0.7	1.1
		5100.895 70	−1.3	1.6
		5110.926 24	2.0	1.1
		5310.159 13	13.1	0.9
		5374.083 25	16.5	2.0
		5403.077 87	16.4	1.1
		5996.201 04	34.9	1.1
		6088.213 96	40.8	1.7
		6767.153 56	52.1	1.0
	HARPS	3039.896 53	−124.3	2.1
		3039.899 01	−125.4	2.1
		3039.901 42	−131.1	2.1
		3306.481 42	−118.9	2.0
		3306.483 46	−120.3	2.0
		3306.485 57	−119.5	2.0
		3429.788 50	−115.1	2.0
		3429.792 10	−115.3	2.0
		3429.795 77	−116.8	2.0
		3429.856 97	−116.4	2.0
		3429.860 64	−116.5	2.0
		3429.864 43	−116.5	2.0
		3521.771 04	−114.7	2.0
		3521.774 80	−116.0	2.0
		3521.778 80	−115.5	2.0
		3523.110 00	−107.5	0.8
		3537.783 18	−115.9	2.0
		3537.787 00	−114.8	2.1
		3537.790 85	−115.5	2.1
		3600.475 66	−111.7	2.0
		3600.479 31	−112.5	2.0

Table 3 – *continued*

HD 156274B	Instrument	Date (JD − 2450000)	RV ($m\,s^{-1}$)	RV error ($m\,s^{-1}$)
		3600.483 26	−112.0	2.0
		3808.762 99	−108.9	2.0
		3808.764 86	−109.5	2.0
		3808.766 69	−109.3	2.0
		3808.784 37	−109.1	2.1
		3808.786 15	−108.3	2.1
		3808.787 93	−108.9	2.0
		3808.805 20	−109.3	2.0
		3808.807 03	−109.1	2.0
		3808.808 86	−107.5	2.0
		3828.813 48	−107.0	2.0
		3828.815 29	−106.9	2.0
		3828.817 03	−107.1	2.0
		3873.657 16	−107.2	2.0
		3873.658 94	−108.3	2.0
		3873.660 69	−107.3	2.0
		3877.676 21	−108.4	2.0
		3877.678 07	−108.8	2.0
		3877.679 83	−107.9	2.0
		3896.757 31	−103.2	2.1
		3896.759 08	−103.0	2.1
		3896.760 77	−103.7	2.1
		3915.849 89	−106.3	2.0
		3915.851 69	−107.8	2.0
		3915.853 43	−105.5	2.0
		3988.627 57	−104.6	2.1
		3988.629 34	−103.3	2.1
		3988.631 17	−104.7	2.0
		4161.801 81	−100.4	2.1
		4161.803 56	−99.6	2.1
		4161.805 31	−98.8	2.1
		4192.865 33	−100.3	2.0
		4192.867 08	−100.0	2.0
		4192.868 83	−99.5	2.0
		4203.893 16	−100.0	2.0
		4203.894 89	−102.0	2.0
		4203.896 65	−101.3	2.0
		4246.683 53	−96.1	2.1
		4246.685 28	−96.7	2.1
		4246.687 03	−96.7	2.1
		4290.697 83	−97.1	2.2
		4290.699 97	−96.3	2.2
		4290.701 67	−96.7	2.3
		4312.595 89	−95.0	2.0
		4312.597 65	−96.1	2.1
		4312.599 44	−95.8	2.0
		4339.531 13	−94.1	2.0
		4339.532 88	−95.0	2.0
		4339.534 66	−94.9	2.0
		4350.552 36	−96.1	2.0
		4350.554 12	−94.4	2.1
		4350.555 87	−95.8	2.1
HD 158783	Instrument	Date (JD − 2450000)	RV ($m\,s^{-1}$)	RV error ($m\,s^{-1}$)
	UCLES	915.258 87	−1160.7	5.3
		1384.060 35	−891.6	1.8
		1386.870 73	−871.0	1.8
		1410.891 83	−828.4	2.2
		1413.892 04	−821.8	1.7
		1630.308 34	−320.9	2.0
		1683.089 59	−182.0	2.2
		1684.135 87	−185.8	2.2

Table 3 – *continued*

HD 158783	Instrument	Date (JD − 2450000)	RV ($m\,s^{-1}$)	RV error ($m\,s^{-1}$)
		1706.102 37	−107.5	2.1
		1718.114 25	−82.0	2.0
		1742.905 40	−6.2	2.0
		1743.919 51	−9.8	2.4
		1745.050 91	0.8	2.1
		1827.908 31	251.1	2.2
		1828.882 93	246.5	2.5
		1829.885 74	251.8	2.8
		1984.258 18	725.0	3.0
		2009.185 80	826.7	2.7
		2061.109 05	985.6	2.3
		2091.974 55	1090.1	2.1
		2126.969 48	1188.2	1.9
		2711.308 21	2693.2	1.4
		6793.238 33	1587.9	1.2
		6794.204 68	1598.6	1.0
HD 162255	Instrument	Date (JD − 2450000)	RV ($m\,s^{-1}$)	RV error ($m\,s^{-1}$)
	UCLES	1002.052 44	6218.0	4.7
		1382.996 01	1036.8	2.0
		1410.969 27	−11 071.1	2.9
		1630.294 29	13 912.1	2.1
		1684.174 16	16 122.8	2.6
		1718.137 92	0.0	1.9
		1742.940 71	−3974.7	2.2
		1744.027 28	−6307.1	1.9
		1766.962 37	1667.6	2.1
		1827.926 94	16 187.1	2.4
		1984.282 28	−7283.5	2.9
		2061.138 15	12 969.8	2.0
		2091.995 01	−14 472.3	2.3
		2127.032 19	−4974.4	1.6
HD 169586	Instrument	Date (JD − 2450000)	RV ($m\,s^{-1}$)	RV error ($m\,s^{-1}$)
	UCLES	917.303 25	−6740.6	6.5
		1120.892 31	−5470.6	4.6
		1683.110 45	−892.4	5.0
		1744.018 38	−152.0	5.3
		1745.089 61	−160.5	5.0
		1766.966 49	0.0	5.4
		2061.142 42	3385.1	7.1
		2711.319 87	863.5	11.2
		2748.209 56	−508.7	10.2
		5374.134 37	6244.4	7.2
HD 175345	Instrument	Date (JD − 2450000)	RV ($m\,s^{-1}$)	RV error ($m\,s^{-1}$)
	UCLES	1119.922 72	−57.5	3.0
		1387.197 87	3319.5	3.0
		1410.950 38	1550.7	3.5
		1472.912 36	−3628.9	3.2
		1683.129 96	4575.2	4.3
		1706.157 76	2859.0	8.9
		1718.144 93	1940.2	3.3
		1742.956 21	73.7	4.1
		1743.996 65	0.0	3.8
		1745.095 75	−78.5	4.4
		1827.949 94	−9067.6	3.5
		1984.290 80	5441.5	5.1
		2061.156 04	−367.2	5.0
		2092.015 01	−3053.1	4.1
		2127.060 57	−7052.3	3.1
		2748.205 73	−6569.9	5.3

semi-amplitude of 32 $m\,s^{-1}$, which if it were a genuine Doppler signal, would give rise to a planet with mass around 1 M_J. The addition of this signal can serve to decrease the rms by a factor 2.

HD 121384: Classified as G8V (Gray et al. 2006), and listed in Dommanget & Nys (1994) along with a common $V = 13$ proper-motion companion (position angle 45°, separation 31 arcsec, 1941), this star is identified by Oudmaijer et al. (1992) and by Aumann & Probst (1991) as having a Vega-like IR excess. Bond et al. (2006) find an [Fe/H] value of -0.40 ± 0.07 dex, in excellent agreement with the value found by Casagrande et al. (2011) of −0.39 dex, yet in good agreement within the uncertainties with Bond et al. (2006). The colour and magnitude are well fit by 7–10 Gyr isochrones indicating that the primary component is indeed evolving away from the main sequence – a view further evidenced by the low level of R'_{HK} activity (−5.22; Henry et al. 1996). Accordingly its stellar mass is estimated at $0.98 \pm 0.10\,M_\odot$. The 179-d period is sharply defined by the broad phase coverage and the Keplerian solution, albeit with a relatively large rms of 15.1 $m\,s^{-1}$. The data indicate that there is a $0.17 \pm 0.01\,M_\odot$ companion orbiting with an eccentricity of 0.84. An eccentricity of this magnitude (Fig. 4) places this binary in the extreme upper tail of the eccentricity distribution for systems with periods <1000 d (Duquennoy & Mayor 1991, fig. 6a) and when combined with the window function, makes the detection of this signal from periodogram analysis alone very difficult (see Fig. 2).

HD 131923: The colour–magnitude location is well fit by 9–12 Gyr isochrones with metallicities of −0.05 and 0.06 dex for Bond et al. (2006) and Casagrande et al. (2011), respectively. These close to solar values suggest that this high proper-motion G4V star (Gray et al. 2006) is starting to evolve away from the main sequence; by contrast, the age inferred from its R'_{HK} index (−4.90; Henry et al. 1996) is only ∼4 Gyr. Given the monotonic variation in RV measurements, the period is poorly defined, though a 7496-d Keplerian solution emerges with an eccentricity of 0.72. The rms for the fit is above average (∼9 $m\,s^{-1}$) and this is reflected in a χ^2_υ of 21.8. With an inferred mass for the primary of $1.05 \pm 0.05\,M_\odot$, the orbital parameters translate to a secondary minimum mass of $\sim 0.52 \pm 0.06\,M_\odot$. The star is identified in the HIPPARCOS catalogue as a 'suspected non-single' object.

HD 145825: This G3 dwarf (Torres et al. 2006) again appears to have a metallicity consistent with solar ([Fe/H] = −0.04 and 0.12 dex from Bond et al. 2006 and Casagrande et al. 2011) and isochrone fitting suggests an age under 3 Gyr, which is consistent with the relatively high level of R'_{HK} activity (−4.74; Henry et al. 1996). Consequently, the stellar mass is estimated at $1.03 \pm 0.05\,M_\odot$. Recent RV measurements have improved the phase coverage, leading to a more sharply defined period of 6024 ± 163 d. With a minimum mass of $0.06 \pm 0.01\,M_\odot$, this adds to the list of brown dwarf candidate companions in our sample.

HD 150248: Consistently classified as a G3V (Evans et al. 1957; Houk 1978; Gray et al. 2006), the sub-solar metallicity of [Fe/H] = −0.11 dex from Bond et al. (2006) and −0.13 dex from Casagrande et al. (2011) suggest an age from isochrone fits of ∼7 Gyr, which contrasts with an activity-inferred age of ∼ 4 Gyr (R'_{HK} activity of −4.88 from Henry et al. 1996). A mass of $0.93 \pm 0.05\,M_\odot$ is estimated for the star. The orbital parameters are fairly well defined, with a period of 3272.4 ± 28.7 d and eccentricity of 0.67, relating to a companion with a minimum mass of $0.10 \pm 0.02\,M_J$.

HD 156274B: Listed as a multiple-star system in Dommanget & Nys (1994), comprising four known components: Gl 666A, a G8V (Eggl et al. 2013), Gl666B, an M0 dwarf (separation 7.5 arcsec, 1880), a $V = 12.5$ companion, and a 14.0 companion (respectively, 279°, 41.8 arcsec, 1900; 30°, 47 arcsec, no year). Our RV

measurements indicate that Gl666A is itself a spectroscopic binary. No spectral metallicity was determined but Casagrande et al. (2011) find a metal-poor value of [Fe/H] = −0.40 dex. Such a value demands isochrones of 9–10 Gyr, though the star would appear to be no older than ∼6 Gyr judging from its $R'_{\rm HK}$ index (−4.95; Jenkins et al.) in which case isochrones with metallicities of 0.1–0.2 dex provide complementary fits. These two scenarios translate to a stellar mass estimated at 0.83 ± 0.06$M_{\odot}$. The best-fitting period is found to be 524 years, implying a secondary minimum mass of 0.20 ± 0.03 $M_{\rm J}$, the fit has an rms of 5.95 m s^{-1}, however we note that the uncertainties on the measured quantities from the bootstrap are formal to the solution presented. It is clear that this is the minimum best fit to the data and so the true solution could be very different and therefore properties like the time of periastron passage are essentially unconstrained.

HD 158783: This G3/G5 dwarf (Houk & Cowley 1975) appears to have a metallicity slightly under solar (−0.05 dex from Bond et al. (2006) and 0.05 dex from Casagrande et al. 2011) and isochrone

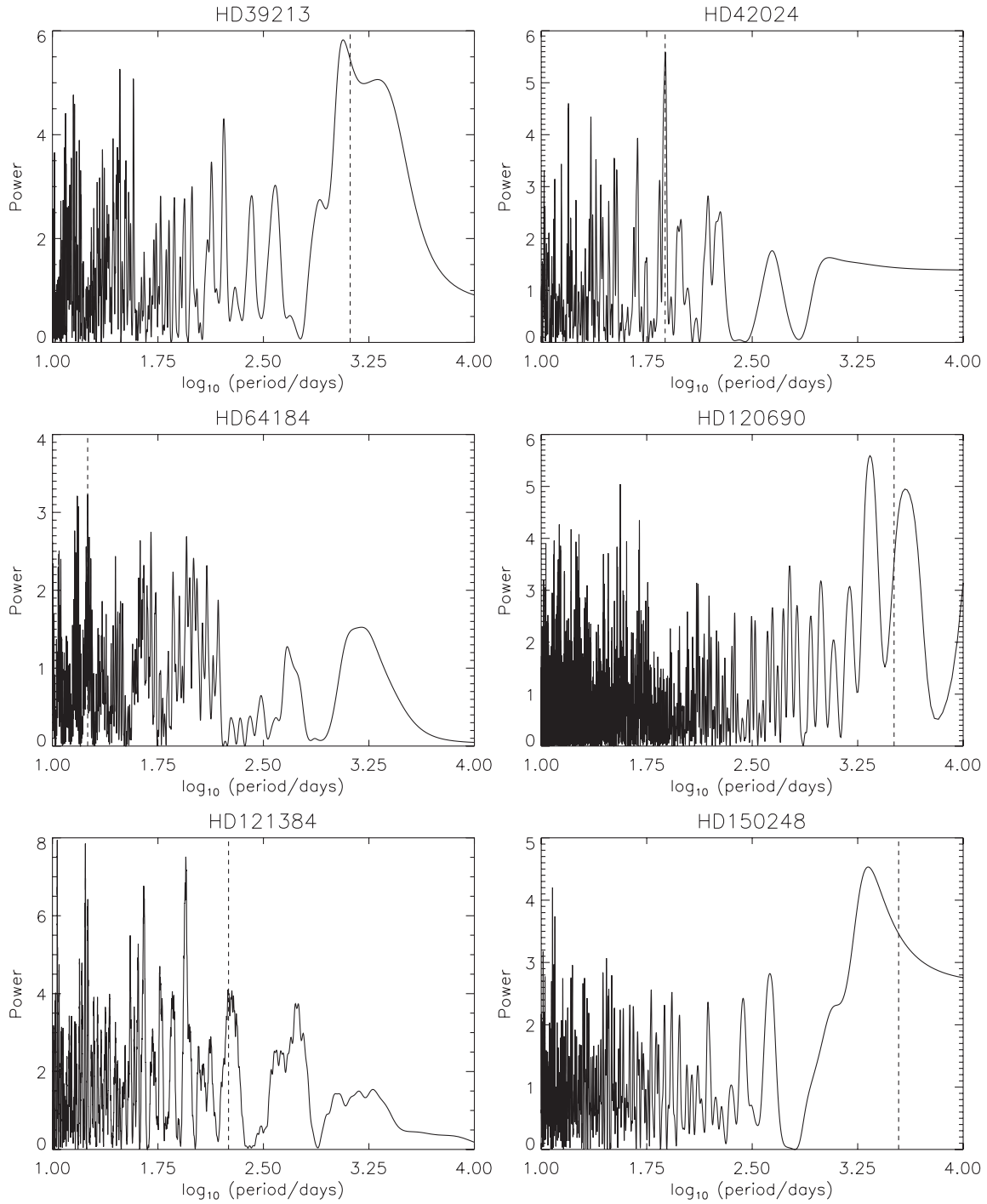

Figure 2. Lomb–Scargle periodograms. These are plots of spectral power against *log* period and are shown for all the stars where the phase coverage of the RV data is nearly a cycle or more. Where the sampling is sparse, aliasing introduces spectral power over a range of frequencies and is particularly marked for HD 64184. The period inferred from the orbital solution in each case is marked with a vertical dashed line.

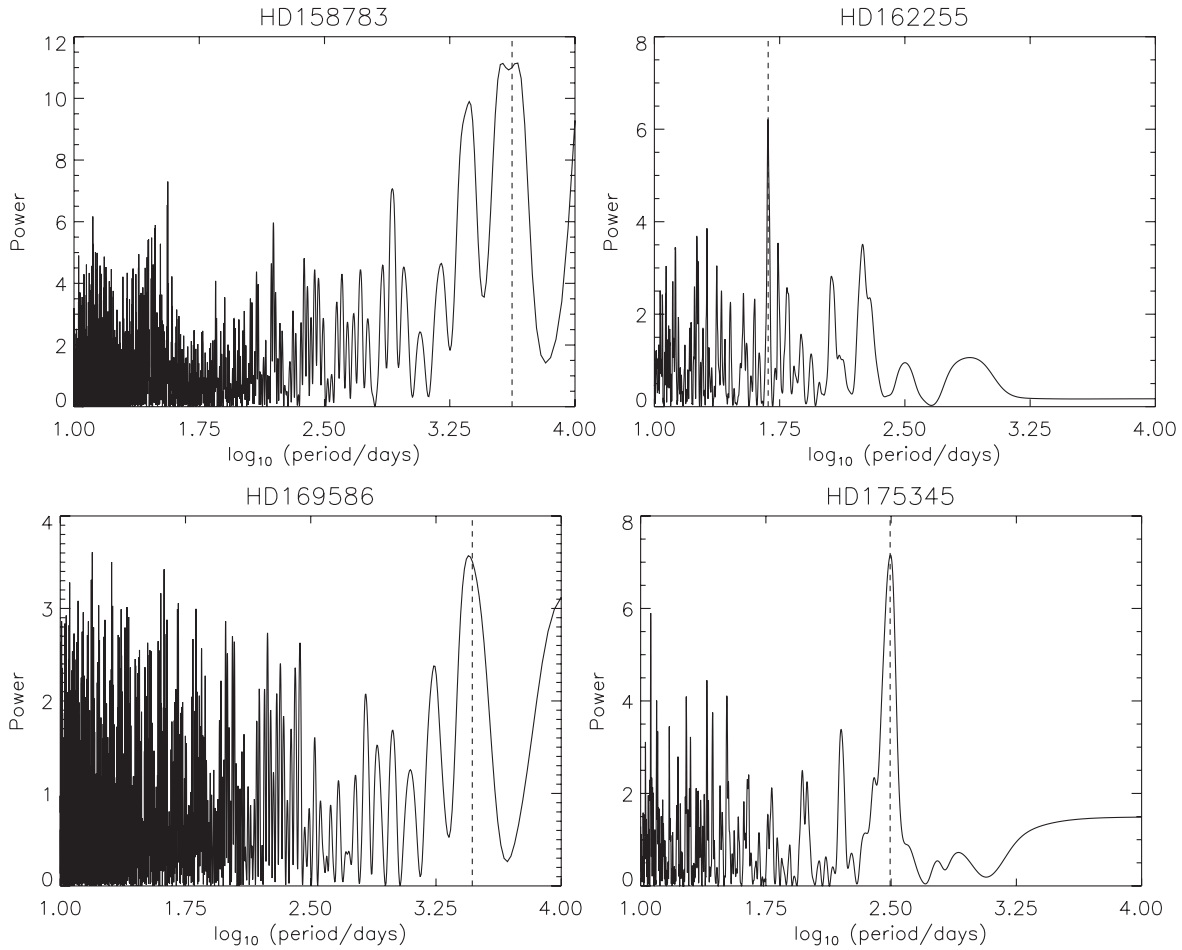

Figure 2 – *continued*

fits demand an age of 8–10 Gyr, significantly above the 4 Gyr age inferred from the star's $R'_{\rm HK}$ index (−4.91; Henry et al. 1996). A stellar mass of 1.04 ± 0.05 $M_\odot$ is inferred. Orbital parameters are tightly defined given the limited phase coverage of the RV measurements and the Keplerian fit is significant at the 20 per cent level. A period of 4534.78 ± 224.92 d and zero eccentricity translate to a secondary minimum mass of 0.20 ± 0.02 $M_\odot$.

HD 162255: Though no $R'_{\rm HK}$ index is given for this G3 dwarf (Houk & Smith-Moore 1988), isochrone fits based on ∼−0.01 dex (Bond et al. 2006) and 0.17 dex (Casagrande et al. 2011) metallicities suggest an age ranging from 5 to 9 Gyr, translating to a stellar mass of 1.12 ± 0.08 $M_\odot$. The eleven RV measurements fold convincingly around a 47.95-d period, indicating a companion minimum mass of 0.333 ± 0.001 $M_\odot$.

HD 169586: This G0V star Houk (1982) appears metal rich ([Fe/H] = 0.32 dex; Casagrande et al. 2011) suggesting an age around 2–4 Gyr, which is in agreement with that derived from the $R'_{\rm HK}$ index (−4.92; Henry et al. 1996); the stellar mass is estimated at 1.25 ± 0.05$M_\odot$. The acquisition of two of the most recent RV measurements has defined a relatively sharp extremum in what was originally a monotonic RV variation so that a 2935-d orbit with an eccentricity of 0.35 appears well constrained. Given that the secondary has a minimum mass of 0.68 ± 0.22 $M_\odot$ (equivalent to an $M_V = 9.4$ companion) contamination of the primary's spectrum has almost certainly taken place, and is possibly a reason why the rms for the fit (60.2 m s^{-1}) is so large, along with the large χ^2_υ. Nevertheless, the existing RV measurements clearly indicate that the primary has one or more companions.

HD 175345: Listed in Dommanget & Nys (1994) as having a $V = 14.2$ proper-motion companion (B 413: 252°, 5.4 arcsec, 1927), our measurements indicate that this G0 dwarf (Houk & Smith-Moore 1988) is itself a spectroscopic binary. There is no $R'_{\rm HK}$ index for this star and the isochrone fits based on its Casagrande et al. (2011) metallicity of [Fe/H] = −0.16 dex gives an age range of 4–9 Gyr along with an inferred mass of 1.05 ± 0.05 $M_\odot$. There is a clear fold of the RV data around a 312-d period so orbital parameters are tightly constrained; however, the residuals are relatively large (rms = 14 m s^{-1}) making the fit statistically poor, even though the χ^2_υ is fairly low (3.44). With a minimum mass of 0.48 ± 0.08 $M_\odot$, (equivalent to $M_V = 9.5$ or brighter) the secondary is again a source of spectral contamination.

The locations of these stars on a HIPPARCOS-based HR diagram, along with a summary of the isochrone fits, are shown in Figs 3(a) and (b), respectively. We also show the distribution of eccentricity versus period in Fig. 4. We find that the companions to HD 121384 and HD 175345 have very high eccentricities for companions with orbital periods below 1000 d, placing them in the extreme upper tail of the distribution in this parameter space. We also find a few of the longer period companions that have not been fully constrained yet due to the limited baseline of the data have moderate to high eccentricity. Although the periods of the orbits could be significantly longer, the eccentricities are rather well constrained with the current

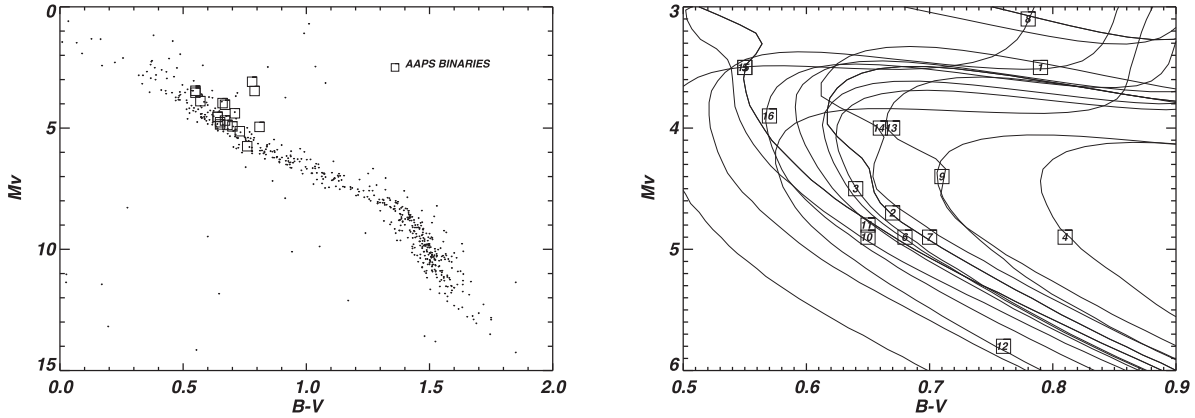

Figure 3. (a) The AAPS binaries are indicated on a colour–magnitude diagram constructed using HIPPARCOS data for solar-neighbourhood stars. (b) Best-fitting isochrones for each star; the numbers assigned to the stars are given in Table 1.

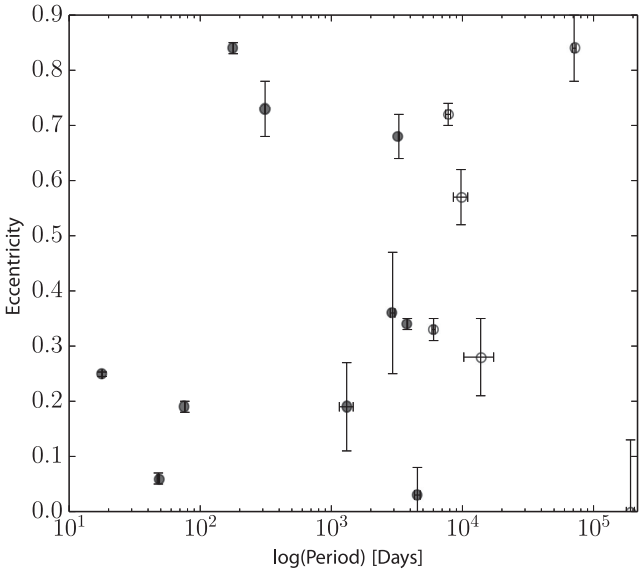

Figure 4. A plot of eccentricity versus period for the AAPS binaries. The binaries represented by filled circles are from Table 2 (i) and have well constrained Keplerian periods; open circles are used for binaries with poorly constrained periods – given in Table 2 (ii).

data in hand, assuming a single Keplerian fit. The one obvious exception is HD 156274B which currently only exhibits a linear trend with velocity over time, and although we fit this will a circular model, this could very well be highly eccentric.

3.2 High-contrast observations

A number of the binaries we have discovered in this work have been followed up using adaptive optics systems to search for direct confirmation of the companions. Obtaining orbital motion from direct images of low-mass companions to bright Sun-like stars, especially when coupled with RV information, can yield dynamical masses for the companions (Liu, Leggett & Chiu 2007). Combining dynamical masses with photometric colours and spectra can allow evolutionary and atmospheric properties to be well constrained and models to be tested (e.g. Dupuy, Liu & Ireland 2009).

In Jenkins et al. (2010) we observed two of the host stars we report new binaries for in this work, HD 25874 and HD 145825. In that work we found contrast ratios of greater than 11 mag at

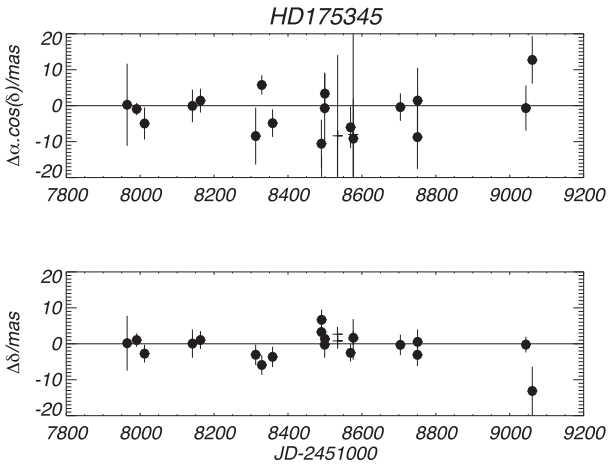

Figure 5. An example astrometric plot of the positional residuals and associated errors for HD 175345.

separations of only 0.5 arcsec using the VLT NAOS CONICA instrument (Rousset et al. 2003) in Simultaneous Differential Imaging mode. Although a tentative detection of the companion around HD 25874 was discussed, further analysis revealed this to be a probable artefact of the reduction and analysis procedure, and therefore no companion detection was conclusively made for either of these stars with mid-T dwarf masses of around 50 M_J or so. Some of the other stars we report companions for are included in our ongoing NACO/NICI imaging campaign.

3.3 HIPPARCOS astrometry

Out of these 16 binaries, 4 (HD 39213, HD 120690, HD 121384, and HD 175345) have well constrained periods in the range 0.5–6 yr, making them suitable candidates for analysis of their HIPPARCOS astrometry. In order to determine if there are any astrometric signatures that would allow us to place additional constraints on our orbital parameters, we extracted the astrometric data from the HIPPARCOS data base (van Leeuwen 2007) and derived positional residuals ($\alpha\cos\delta$, δ). In Fig. 5 we show these with associated errors for HD 175345.

There are no significant variations obvious in the plots for the four candidates, though in the case of HD 175345, periodogram analysis reveals significant power at around 320 d (cf. a 312-d period from RV analysis). Failure, however, of these data to fold around either

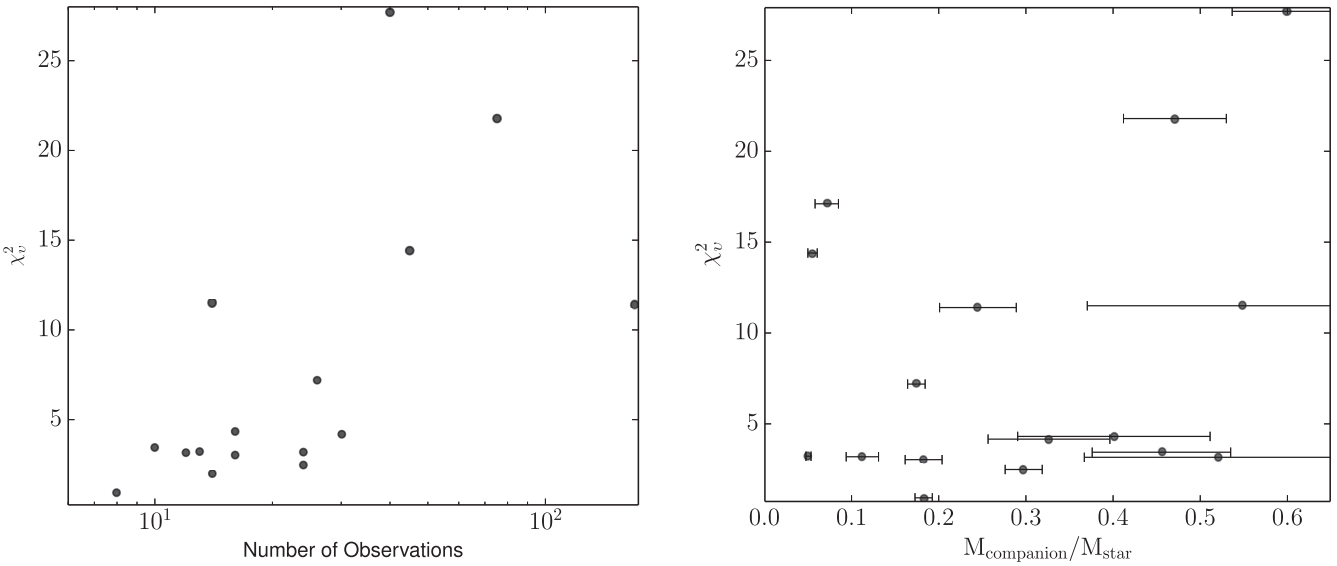

Figure 6. Quality of orbital fit (in terms of the statistical significance attributed to the χ^2_v value) versus (a) the number of observations per star (b) the minimum mass ratio of the system.

period suggests that the spectral power owes more to sampling of the data (which have a strong 300-d element) than to any possible astrometric signature. The significance of the astrometric variations is clearly low and we do not attempt further to constrain our orbital parameters using these data.

3.4 Secondary flux contamination

In those cases where the orbits are fully constrained and the secondary minimum mass is $\sim$0.5M$_\odot$ (HD 18907, HD 26491, HD 120690, HD 131923, HD 169586, and HD 175345), the contribution of the secondary to the overall flux is at least 1 per cent and the signature of this contribution is found in the quality of the orbital solutions: the rms scatter of these stars is generally much higher than the internal measurement uncertainty. The reason for this is that flux from the secondary, which is contaminating the primary's spectrum, will be associated with a different RV at each of the subsequent observations from that when the template spectrum was acquired. The RV fitting process relies on the assumption that the primary's spectrum is modified only by the Doppler shift of the primary and the spectrograph PSF variation. Consequently, less than optimal solutions can be expected when a faint secondary contribution to the primary's spectrum is present at variable Doppler shifts. In essence, the fitting process matching the observed and synthetic spectra would be expected to generate larger measurement errors, and this is the case particularly for HD 169586. Fig. 6 shows how the quality of the orbital solutions – measured by the significance of the fit – varies with the number of observations (plot a) and the binary minimum-mass ratio (plot b). While no correlation appears to be evident between the reduced chi-squared and companion mass ratio, in general, the statistical significance of the fits appear to indicate a marked deterioration as the number of data points increase. This could reflect the fact that these are the systems exhibiting the most stellar flux contamination and therefore they required more observations in order to better constrain their orbits, or, another possibility is that these systems also contain additional companions, either brown dwarfs or planets, that are giving rise to mixed signals that are being manifest once enough RV measurements have been acquired.

Given the precision with which RVs can be obtained by the AAPS, we could speculate that where low $M \sin i$ values yield statistically poor fits (HD 39213, HD 121384), the orbital inclinations are low and that the companions have masses high enough for spectral contamination to be taking place. The large errors in RV measurements for HD 39213 and HD 156274 lend credence to this scenario, though this is not the only explanation. It is also possible that these are multiple systems for which a double-star solution simply is not appropriate. Moreover, enhanced activity in any of these stars (bearing in mind that the $R'_{\rm HK}$ index is merely a 'snapshot' measurement) would mean that the internal errors would not properly reflect the uncertainty in the RV measurements. This is why it is pragmatic to use relatively inactive stars in Doppler searches. For the targets considered here, enhanced activity is unlikely to be the cause: Henry et al. (1996) estimate that 90 per cent of the time a single $R'_{\rm HK}$ measurement for a solar-type star is sufficient to identify correctly if it has an activity greater, or less, than $R'_{\rm HK} = -4.75$, and all but one of the stars have $R'_{\rm HK}$ indices lower than this. Where the measurement errors are low but the orbital solutions are statistically weak (HD 121384 and HD 162255), the most convincing explanation is that these systems comprise more than a single companion.

The effect of binarity on the colour and magnitude of a primary of any age and metallicity can be modelled easily using the Yonsei–Yale isochrone data. Fig. 7 shows the variation in colour and magnitude for a 5.5 Gyr, solar metallicity isochrone ranging in mass from 0.88 to 1.20 M$_\odot$ (solid curve). The effect of adding a secondary is marked by the dotted curves at various mass intervals, with each point representing a secondary companion that increases in mass from 0.5 to 1.0 $M_{\rm p}$ in steps of 0.05 $M_{\rm p}$.

For companions below 0.55 $M_{\rm p}$ the effect of binarity on the colour–magnitude location of the primary is negligible. The effect of a 0.70 $M_{\rm p}$ companion is to make the primary appear redder and brighter by around 0.05 and 0.3 mag, respectively, for a solar-mass star, with slighter larger and smaller values for less massive and more massive primary stars, respectively. Such an effect generally makes the unresolved pair appear older and/or more metal rich;

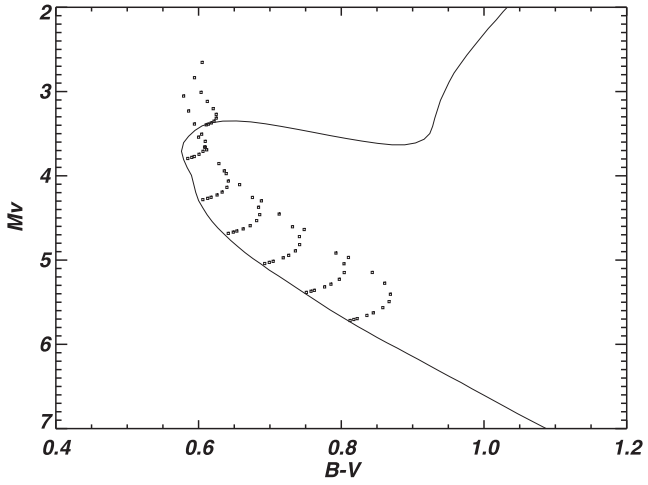

Figure 7. Effect of binarity on the colour and magnitude at 5.5 Gyr for solar metallicity primaries ranging in mass from 0.88 to 1.20 $M_{\odot}$. Secondary mass values increase in 0.05 $M_{\rm p}$ increments from 0.5 to 1.0 $M_{\rm p}$.

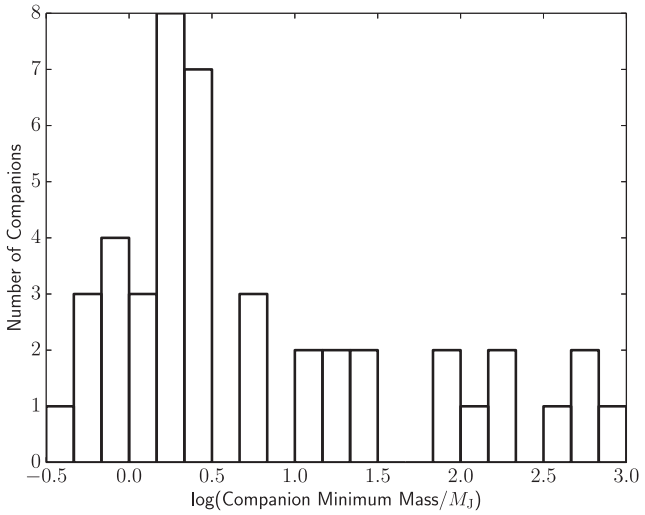

Figure 8. The raw distribution of companion minimum masses uncovered by the AAPS with periods less than 12 years.

however, if the primary itself is evolving away from the main sequence, the companion will make the pair appear 'bluer'. These effects will complicate the process of mass estimation. For example, the presence of a 0.70$M_{\rm p}$ companion translates effectively to a systematic error of $\sim 0.04 M_{\odot}$ in the mass of the primary. This is of the order of the error in mass due to the age–metallicity uncertainties. The orbital solutions indicate binary mass ratios generally significantly less than unity (HD 169586 being the exception) so that the effect of binarity on the determination of the primary mass (and by extension the secondary mass) is negligible. Clearly, for many of the binaries in our sample, the uncertainty in secondary mass is due principally to poorly constrained orbital parameters.

3.5 Mass distribution

The binaries and planetary companions to solar-type stars reported by the AAPS provide an opportunity to examine, from a single RV survey, the distribution of $M \sin i$ values for a mass regime extending from Jovian through brown dwarf to sub-solar in value.

In order to derive a more meaningful distribution of minimum-mass ratios, we need to impose a period cut-off on both the planetary and binary companions so that we count only those companions within a certain distance of the primary stars. As a rule, planetary candidates are announced when the phase coverage of the RV data are close to one orbital period. For the AAPS, which has been operating since 1998, we can say that the inventory of exoplanet candidates orbiting with periods up to 12 years (i.e. out to around the orbit of Jupiter in the Solar system) is reasonably complete down to the level permitted by a Doppler precision of $\sim$3 m s^{-1}, i.e. complete for Jupiter-mass objects and above. Brown dwarf and low-mass stellar companions induce larger reflex velocities making them easier to detect over a greater range of distances and periods. In order to compare directly with Duquennoy & Mayor (1991), 6 out of the 16 binaries have periods greater than 12 years and these need to be excluded from our count.

10 remaining binaries out of a sample of 178 stars is around half of that expected from the period distribution given in fig. 13 of Raghavan et al. (2010), when normalized by the multiplicity fraction, though there are several reasons for this. First, our sample excludes all *known* short-period spectroscopic binaries with separations less than 2 arcsec; secondly, all binaries beyond 2 arcsec detected using HIPPARCOS data are excluded from our sample; thirdly, 'double-lined' spectrum binaries are immediately removed as soon as they are recognized; fourthly, our requirement for the AAPS target stars to have an $R'_{\rm HK}$ index below -4.5 has the effect of filtering out some short-period, chromospherically active binaries – RS CVn/W UMa types for example – though admittedly these are few in number. The observed distribution in minimum masses, corrected for completeness for periods up to 12 years, is shown in Fig. 8.

The main features seen in this $P < 12$ yr distribution are (i) a sub-stellar companion mass function rising strongly below 10 $M_{\rm J}$, (ii) a comparatively flat distribution of stellar companions, and (iii) a region from $\sim$20 to 70 $M_{\rm J}$ (corresponding to the brown dwarf regime) where relatively few objects are found despite a selection bias in the observations making them easier to detect than planets. Note that although objects do exist in this part of the parameter space (e.g. Jenkins et al. 2009), the term brown dwarf desert was given to highlight the relative paucity in comparison to planets and stellar objects (Marcy & Butler 2000). Such features accord with RV observations elsewhere: the CORALIE, Keck, and Lick surveys all report the same form of sub-stellar function while the 'flat' stellar distribution mirrors that seen in Duquennoy & Mayor (1991, fig. 11). This similarity comes about despite the fact that the various RV surveys work with different samples and operating strategies. The form of the distribution of planetary and stellar companions is considered to reflect the different formation mechanisms for these two populations (respectively accretion in dissipative circumstellar discs and gravitational instabilities in collapsing cloud fragments) and their consequent evolution. The relatively small number of brown dwarf companions has been noted elsewhere (for example Halbwachs et al. 2000; Butler et al. 2001; McCarthy 2001) and may be a reflection of a formation mechanism different again from that of stars or planets, though Armitage & Bonnell (2002) argue that its existence is a consequence of orbital migration of brown dwarfs within an evolving protostellar disc.

The question arises as to what effect a correction for inclination would have on the observed distribution. The simplest (crudest) correction is to scale masses up by a factor of $1/\langle \sin i \rangle$. This does not alter the form of the distribution, nor in this case the total

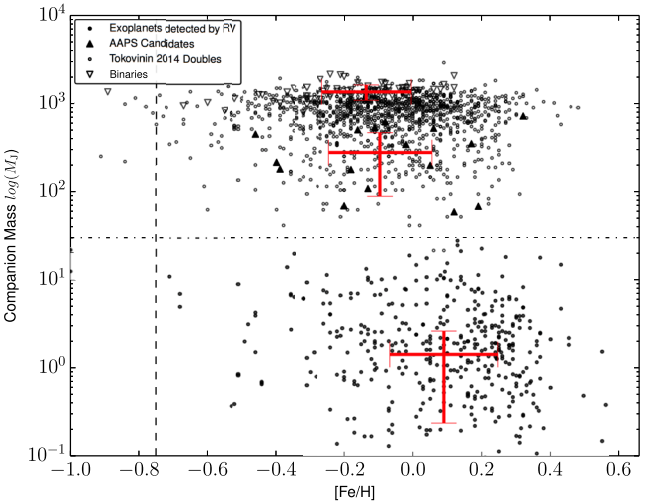

Figure 9. Metallicity–mass distribution. Filled circles correspond to exoplanets with $1.5\,M_J < M < 5.0\,M_J$, discovered using the RV technique, open triangles correspond to binary stars from Halbwachs, Mayor & Udry (2012) and Duquennoy & Mayor (1991), filled triangles show our AAPS candidates, and open circles show the distribution for doubles reported by Tokovinin (2014). The metallicities were obtained from Casagrande et al. (2011). The horizontal and vertical lines mark the approximate planet–brown dwarf boundary and the extreme lower tail of the Tokovinin binary distribution, respectively. The cross-hairs mark the sample medians for the planets, AAPS candidates, and the Tokovinin (2014) binaries, increasing in mass, respectively.

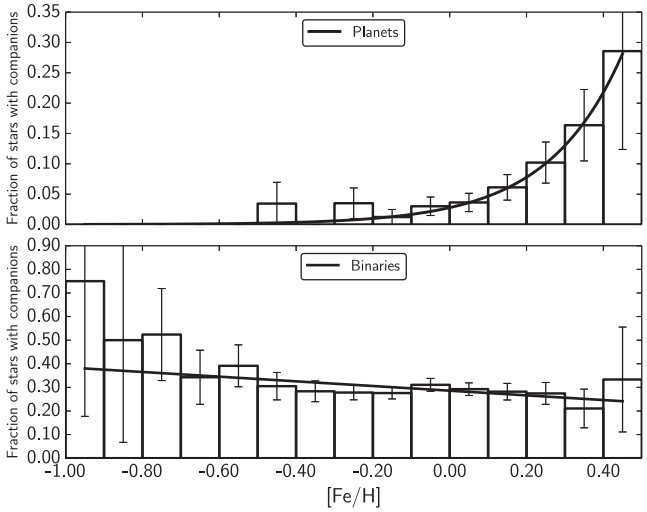

Figure 10. The metallicity distribution of exoplanet (upper panel) and binary (lower panel) companions. The best-fitting model distributions are also shown in the plots, where a power law is used for the exoplanet sample, and a linear function is used to model the binary distribution.

number of objects that can be regarded as brown dwarf candidates – just those objects out of the survey that can be regarded as such. Clearly, a knowledge of the precise form of the mass distribution for this (or any) RV survey is precluded until inclinations can be determined accurately via sub-milliarcsecond astrometric surveys such as *GAIA* (Sozzetti et al. 2001) and SIM (Sozzetti et al. 2002), though it would take a remarkable confluence of inclinations for the objects uncovered by the AAPS to alter the underlying distribution of masses. Indeed, recent attempts have been made to recover the 'true' mass distribution (Lopez & Jenkins 2012), with very few of the sub-10 M_J objects moving above this mass limit.

3.6 Metallicity–mass distribution

One of the most interesting features to emerge from the early study of exoplanets is the dependence of gas giants to be found orbiting stars with supersolar metallicities (Gonzalez 1997; Fischer & Valenti 2005; Sousa et al. 2011). This result is a key prediction of the core accretion scenario for planet formation (Ida & Lin 2004; Mordasini et al. 2012). However, it seems that this bias towards the most metal-rich stars is only found for gas giants and not lower mass rocky planets (Udry et al. 2007; Buchhave et al. 2012; Jenkins et al. 2013a). Therefore, given there is a clear mass dependence as a function of metallicity, it is interesting to test what the metallicity distribution looks like for binaries drawn from a representative sample.

In Fig. 9 we show the distribution in the metallicity–mass plane of planets, brown dwarfs, and stellar binaries that have been detected mostly by the RV method, with a large clutch of the stellar binaries being drawn from the sample of F, G, and K stars from Tokovinin (2014). The iron abundances used in this plot were taken from high-resolution spectral analysis where possible, generally from the published papers for the detected exoplanets, with the Tokovinin (2014) primary star metallicities being drawn from Casagrande et al. (2011). The giant planet metallicity bias discussed above is evident here, where the sample mean cross-hairs are clearly offset from the sample means at higher masses (i.e. above the horizontal dot–dashed line). The brown dwarf and stellar binaries have mean values in good agreement with each other, both with sub-solar values, in comparison to the exoplanet primary mean distribution that is significantly above the solar value.

In Fig. 10 we show the distribution of exoplanets and binaries as a function of primary star metallicity. We used the large sample of Fischer & Valenti (2005) for the exoplanet distribution and again the Tokovinin (2014) sample for the binary population. The biases in both of these samples are discussed in each of the works, yet they are large enough and have been examined well enough that they can be thought of as good representations of their respective field populations. The full Tokovinin (2014) sample was not included since we wanted to maintain metallicity homogeneity and also we aimed for a direct overlap in orbital separation with the exoplanet sample, meaning we only included binary companions with orbital periods out to 4 years. For metallicity homogeneity, we cross-matched the sub-4 year sample with the Casagrande et al. (2011) catalogue of metallicities, leaving a total of 874 binaries or multiple stars, out of the complete 3936 sample.

As was shown in Fischer & Valenti (2005), the distribution of exoplanets follows a power law where the percentage of stars with giant planets increases as a function of metallicity. After constructing a similar histogram of values to that in Fischer & Valenti (2005), we find a power law described by an amplitude of 0.028 ± 0.002 and an index of 2.23 ± 0.09, which we represent by the dashed black curve in the plot. Beyond around a solar metallicity, the increase in planet hosting fraction rises steeply, possibly accelerating beyond a value of $+0.2$ dex in metallicity (Sousa et al. 2011).

The distribution of binaries on the other hand is extremely flat across all the metallicity range, within the uncertainties, with the fraction found to be 43 ± 4 per cent, in excellent agreement with Raghavan et al. (2010). The best-fit-weighted linear function is shown in the figure and has values for the gradient (b) and offset

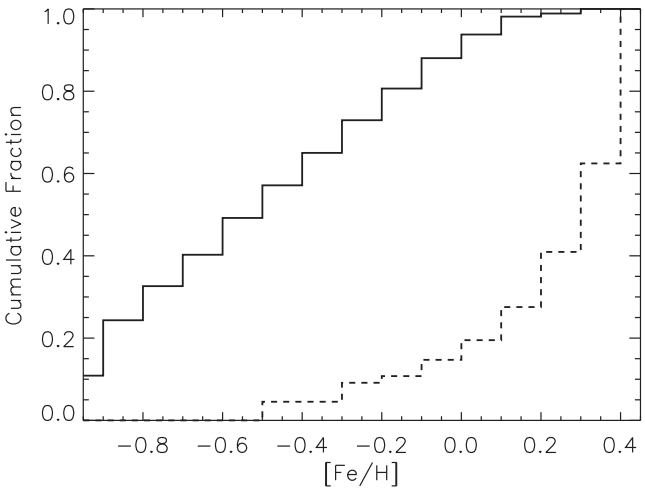

Figure 11. The cumulative fraction of the binary fraction distribution (solid curve) and the exoplanet fraction distribution (dashed curve).

(*a*) of 0.286 ± 0.011 and −0.099 ± 0.044, respectively. These parameters are fairly insensitive to different bin widths, therefore, it is clear that the binarity fraction as a function of metallicity is significantly different to the planetary system fraction.

We investigated if there is any dependence on the binary fraction with orbital separation by constructing the same distribution on the sample of binaries with orbital periods longer than 4 years, and on the full sample regardless of orbital period. We found no significant differences between the distributions; however, we do note a small drop in the fraction of binaries in the metal-poor regime ($-0.8 \leq$ [Fe/H] ≤ -0.5) for the longer period sample. Although it still agrees with a flat distribution within the uncertainties, in future it may be worthwhile to revisit this regime with more binaries in these bins to see if this drop in fraction becomes significant, which would indicate that there is a dependence of the binary fraction with separation as a function of metallicity.

In Fig. 11 we show the cumulative fraction between the binary fraction and the exoplanet fraction as a function of metallicity. The early rise at low metallicities in the binary fraction is apparent, along with the rapid rise at the high-metallicity end for the exoplanet fraction. We find that the largest disparity between the two populations occurs around 0.15 dex in metallicity, a little over solar metallicity, where the planet fraction begins to significantly increase. A Kolmogorov–Smirnov test yields a D-statistic of 0.733 here, relating to a probability of the null hypothesis of 2.377×10^{-2} per cent.

Gao et al. (2014) show that the fraction of binaries with orbital periods of less than 1000 d dramatically falls in the metal-rich regime when they split their Sloan Digital Sky Survey and LAMOST FGK star samples up into three different metallicity bins. They find a total binary fraction of 43 ± 2 per cent, again in excellent agreement with what we find here, but they calculate binary fractions of 56 ± 5 per cent, 56 ± 3 per cent, and 30 ± 5.7 per cent for metallicities ([Fe/H]) of <-1.1, -1.1 to <-0.6, and ≥ -0.6, respectively, indicating a drop in the fraction of binaries in the most metal-rich region. Although this is an indication of a higher fraction of binaries near our metallicity lower limit, within the uncertainties the distribution is still flat (similar to the result reported in Raghavan et al. 2010). Therefore, we cannot confirm if such a binary fraction change exists, a change that is also recovered by some models (e.g. Machida et al. 2009).

Bate (2014) studied the effects of changes of the metallicity on their star formation models, assuming the dust opacity scales linearly with metallicity across a range of metallicities from 1/3rd solar to three times solar metallicity. He finds no significant changes in the multiplicity fraction with metallicity, suggesting gas opacity does not overtly change the large-scale properties of star formation from the fragmentation of giant molecular clouds. Furthermore, he also finds no dependence with metallicity on the orbital separation of binaries and higher order multiples, as we find here. Given that recent works have shown that the cooling times in protoplanetary discs increase as a function of metallicity, meaning suppression of disc fragmentation in the super metal-rich regime (e.g. Cai et al. 2006), we might expect that if FGK star secondaries formed primarily through fragmentation of the protoplanetary disc, there would be a strong dependence of the binary fraction with metallicity. As this does not appear to be the case, then a flat distribution of binary fraction with metallicity suggests that these close binaries predominantly form through fragmentation of the giant molecular cloud that also formed the primary star.

3.7 Summary

Our target sample of 178 solar-type stars has revealed that ∼10 per cent are spectroscopic binaries. Orbital solutions indicate that two systems potentially have brown dwarf companions and another two could have eccentricities that place them in the extreme upper tail of the eccentricity distribution for binaries with periods less than 1000 d. The systems with the largest quantity of data points appear to generate the least robust orbital solutions, which could owe to secondary flux contamination of the template spectra, and hence the necessity to garner more data to constrain their solutions. When the RV measurement errors are low, yet the Keplerian solutions have low significance, the most likely scenario is a multiple-star system. HIPPARCOS astrometry was examined in an attempt to constrain our orbital parameters; however, no significant astrometric variation could be discerned in the positional residuals. The distribution of companion masses was examined for both the binaries and candidate exoplanets detected by the AAPS. For periods up to 12 years the 'steep' planetary and 'flat' binary mass distributions mirror those seen by other surveys. Over a time-scale equivalent to one orbital period of Jupiter, upwards of 30 exoplanet detections can be expected from our original sample of 178 stars. The discovery of these 16 AAPS binaries from a sample of solar-type stars selected to have no resolvable or known SB companions is a reminder that the data for even the relatively bright southern stars remain far from complete.

Finally, analysis of the metallicity–mass plane from planetary companions all the way up to stellar companions reveals a stark difference in the mean metallicities of these populations, with planets orbiting stars more metal-rich than stellar companions, in general. The fraction that host these companions as a function of metallicity is also different, with the binary fraction being found to be flat (43 ± 4 per cent) in the metallicity range between −1.0 and 0.6 dex. This is in contrast to the fraction of stars hosting giant planetary systems, which has a very low fraction until around a solar metallicity, at which point the fraction rises steeply following a power law. The flat binary fraction across this wide range of metallicities is in agreement with recent hydrodynamical simulations of star formation through fragmentation of giant molecular clouds. Such a result suggests that this is the dominant formation mechanism for FGK-type binaries and not fragmentation of the protoplanetary disc that was left over from the formation of the primary star.

ACKNOWLEDGEMENTS

We acknowledge funding by CATA-Basal grant (PB06, Conicyt), from Fondecyt through grant 3110004, and partial support from Centro de Astrofísica FONDAP 15010003, the GEMINI-CONICYT FUND and from the Comité Mixto ESO-GOBIERNO DE CHILE. (JSJ). We thank the support of CONICYT-PFCHA/Doctorado Nacional-Chile (MD). We further acknowledge Australian governmental support of the Anglo-Australian Telescope as part of the Department of Industry and Science (CGT, BC) and NSF grant AST-9988087 (RPB). We also thank David Soderblom for granting the use of Ca II H&K spectra taken at CTIO. This research has made use of the SIMBAD data base, operated at CDS, Strasbourg, France.

REFERENCES

Abt H. A., Gomez A. E., Levy S. G., 1990, ApJS, 74, 551
Anglada-Escudé G. et al., 2014, MNRAS, 443, 89
Armitage P. J., Bonnell I. A., 2002, MNRAS, 330, L11
Aumann H. H., Probst R. G., 1991, ApJ, 368, 264
Baraffe I., Chabrier G., Allard F., Hauschildt P. H., 1998, A&A, 337, 403
Baranne A. et al., 1996, A&A, 119, 373
Bate M., 2014, MNRAS, 442, 285
Bond J. C., Tinney C. G., Butler R. P., Jones H. R. A., Marcy G. W., Penny A. J., Carter B. D., 2006, MNRAS, 370, 163
Bouchy F., Pepe F., Queloz D., 2001, A&A, 374, 733
Buchhave L. A. et al., 2012, Nature, 486, 375
Butler R. P., Marcy G. W., Williams E., McCarthy C., Dosanjh P., Vogt S. S., 1996, PASP, 108, 500
Butler R. P., Tinney C. G., Marcy G. W., Jones H. R. A., Penny A. J., Apps K., 2001, ApJ, 555, 410
Cai K., Durisen R. H., Michael S., Boley A. C., Mejía A. C., Pickett M. K., D'Alessio P., 2006, ApJ, 636, 149
Casagrande L., Schonrich R., Asplund M., Cassisi S., Ramírez I., Meléndez J., Bensby T., Feltzing S., 2011, A&A, 530, 138
Decin G., Dominik C., Malfait K., Mayor M., Waelkens C., 2000, A&A, 357, 533
Dommanget J., Nys O., 1994, Commun. Obser. R. Belg., 115, 1
Dupuy T. J., Liu M. C., Ireland M. J., 2009, ApJ, 692, 729
Duquennoy A., Mayor M., 1991, A&A, 248, 485
Eggl S., Pilat-Lohinger E., Funk B., Georgakarakos N., Haghighipour N., 2013, MNRAS, 428, 3104
Evans D. S., 1964, R. Greenwich Obser. Bull., 85, 207
Evans D. S., Menzies A., Stoy R. H., 1957, MNRAS, 117, 534
Fischer D. A., Marcy G. W., 1992, ApJ, 396, 178
Fischer D. A., Valenti J., 2005, ApJ, 622, 1102
Gao S., Liu C., Zhang X., Justham S., Deng L., Yang M., 2014, ApJ, 788, 37
Gonzalez G., 1997, MNRAS, 285, 403
Gray R. O., Corbally C. J., Garrison R. F., McFadden M. T., Bubar E. J., McGahee C. E., O'Donoghue A. A., Knox E. R., 2006, AJ, 132, 161G
Halbwachs J. L., Arenou F., Mayor M., Udry S., Queloz D., 2000, A&A, 355, 581
Halbwachs J. L., Mayor M., Udry S., 2003, MNRAS, 422, 14
Henry T. J., Soderblom D. R., Donahue R. A., Baliunas S. L., 1996, AJ, 111, 439
Horne J. H., Baliunas S. L., 1986, ApJ, 302, 757
Houk N., 1978, Michigan Catalogue of Two-dimensional Spectral Types for the HD Stars, Volume 2. Department of Astronomy, Univ. Michigan, Ann Arbor, MI
Houk N., 1982, Michigan Catalogue of Two-dimensional Spectral Types for the HD Stars, Volume 3. Department of Astronomy, Univ. Michigan, Ann Arbor, MI
Houk N., Cowley A. P., 1975, Michigan Catalogue of Two-dimensional Spectral Types for the HD Stars, Volume 1. Department of Astronomy, Univ. Michigan, Ann Arbor, MI
Houk N., Smith-Moore M., 1988, Michigan Catalogue of Two-dimensional Spectral Types for the HD Stars, Volume 4. Department of Astronomy, Univ. Michigan, Ann Arbor, MI
Ida S., Lin D. N. C., 2004, ApJ, 616, 567
Jenkins J. S., Tuomi M., 2014, ApJ, 794, 110
Jenkins J. S. et al., 2006, MNRAS, 372, 163
Jenkins J. S., Jones H. R. A., Pavlenko Y., Pinfield D. J., Barnes J. R., Lyubchik Y., 2008, A&A, 485, 571
Jenkins J. S. et al., 2009, MNRAS, 398, 911
Jenkins J. S. et al., 2010, MNRAS, 372, 163
Jenkins J. S. et al., 2011, A&A, 531, 8
Jenkins J. S. et al., 2013a, ApJ, 766, 67
Jenkins J. S., Tuomi M., Brasser R., Ivanyuk O., Murgas F., 2013b, ApJ, 771, 41
Jones H. R. A., Paul Butler R., Tinney C. G., Marcy G. W., Penny A. J., McCarthy C., Carter B. D., Pourbaix D., 2002a, MNRAS, 333, 871
Jones H. R. A., Paul Butler R., Marcy G. W., Tinney C. G., Penny A. J., McCarthy C., Carter B. D., 2002b, MNRAS, 337, 1170
Liu M. C., Leggett S. K., Chiu K., 2007, ApJ, 660, 1507
Lo Curto G. et al., 2010, A&A, 512, A48
Lomb N. R., 1976, Ap&SS, 39, 447
Lopez S., Jenkins J. S., 2012, ApJ, 756, 177
Lovis C., Pepe F., 2007, A&A, 468, 1115
McCarthy C., 1995, M.S. thesis, San Francisco State Univ.
McCarthy C., 2001, PhD thesis, Univ. California Los Angeles
Machida M. N., Omukai K., Matsumoto T, Inutsuka I., 2009, MNRAS, 399, 1255
Mamajek E. E., Hillenbrand L. A., 2008, ApJ, 687, 1264
Marcy G. W., Butler R. P., 2000, PASP, 112, 137
Mason B. D., Gies D. R., Hartkopf W. I., Bagnuolo W. G., Brummelaar T. T., McAlister H. A., 1998, AJ, 115, 821
Mordasini C., Alibert Y., Benz W., Klahr H., Henning T., 2012, A&A, 541, 97
Nidever D. L., Marcy G. W., Butler R. P., Fischer D. A., Vogt S. S., 2002, ApJS, 141, 503
O'Toole S. J., Tinney C. G., Jones H. R. A., Butler R. P., Marcy G. W., Carter B., Bailey J., 2009, MNRAS, 392, 641
Oudmaijer R. D., van der Veen W. E. C. J., Waters L. B. F. M., Trams N. R., Waelkens C., Engelsman E., 1992, A&AS, 96, 625
Pepe F., Mayor M., Galland F., Naef D., Queloz D., Santos N. C., Udry S., Burnet M., 2002, A&A, 388, 632
Perrin M.-N., Cayrel de Strobel G., Dennefeld M., 1988, A&A, 191, 237
Preibisch T., Balega Y., Hofmann K., Weigelt G., Zinnecker H., 1999, New Astron., 4, 531
Raghavan D. et al., 1999, ApJS, 190, 1
Rousset G. et al., 2003, SPIE, 4839, 140
Scargle J. D., 1982, ApJ, 263, 835
Soderblom D. R., Duncan D. K., Johnson D. R. H., 1991, ApJ, 375, 722
Sousa S., Santos N. C., Israelian G., Mayor M., Udry S., 2011, A&A, 533, 141
Sozzetti A., Casertano S., Lattanzi M. G., Spagna A., 2001, A&A, 373, L21
Sozzetti A., Casertano S., Brown R. A., Lattanzi M. G., 2002, PASP, 114, 1173
Tinney C. G., McCarthy C., Jones H. R. A., Butler R. P., Carter B. D., Marcy G. W., Penny A. J., 2001, MNRAS, 332, 759
Tokovinin A., 2014, AJ, 147, 86
Torres C. A. O., Quast G. R., Da Silva L., De La Reza R., Melo C. H. F., Sterzik M., 2006, A&A, 460, 695
Udry S. et al., 2007, A&A, 469, L43
van Leeuwen F., 2007, A&A, 474, 653
Vogt S. S., Butler R. P., Rivera E. J., Highighipour N., Henry G. W., Williamson M. H., 2010, ApJ, 723, 954
Wittenmyer R. A. et al., 2014, ApJ, 791, 114
Yi S., Demarque P., Kim Y., Lee Y., Ree C. H., Lejeune T., Barnes S., 2001, ApJS, 136, 417

This paper has been typeset from a TEX/LATEX file prepared by the author.